Earth Planet. Sci. Lett. 648 (2024) 119084

Contents lists available at ScienceDirect

Earth and Planetary Science Letters

journal homepage: www.elsevier.com/locate/epsl

Low total REE zircon formed in equilibrium with hornblende in granulitized eclogites: Implications for exhumation rates

Jia-Min Wang [a,*], Daniela Rubatto [b,c], Pierre Lanari [c,b], Yu-Lu Tian [a], Yi Chen [a], Fu-Yuan Wu [a]

[a] State Key Laboratory of Lithospheric and Environmental Coevolution, Institute of Geology and Geophysics, Chinese Academy of Sciences, 100029 Beijing, China
[b] Institute of Geological Sciences, University of Bern, Baltzerstrasse 3, CH-3012, Switzerland
[c] Institute of Earth Sciences, University of Lausanne, Géopolis, CH-1015, Lausanne, Switzerland

ARTICLE INFO

Keywords:
Zircon
Rare Earth elements
Eclogite
Amphibole
Exhumation rate
Himalaya

ABSTRACT

Exhumation rates of high-pressure rocks are paramount in determining plate tectonic processes, which requires absolute chronology of metamorphic stages. U-Pb geochronology of zircon and other accessory minerals has proven successful in dating different metamorphic stages, thus constraining geological rates. A common strategy to link U-Pb ages to metamorphic stages uses rare earth element (REE) patterns in the dated minerals. In this study, the changes in the REE composition of accessory and rock-forming minerals in response to changing assemblages have been investigated in granulitized eclogites and gneisses from the Ama Drime Massif, central Himalaya. Phase equilibrium modelling shows that the eclogite-facies assemblage formed at 660–720 °C and 1.6–1.9 GPa (M1), was overprinted at high-pressure granulite-facies (M2) and then ultra-high temperature conditions of >900 °C and 0.8–1.1 GPa (M3) and finally re-equilibrated at conditions of 780–810 °C and 0.8–1.0 GPa (M4). In the countryrock orthogneisses, monazite records partial resetting during granulite-facies overprinting at 26–19 Ma and melt crystallisation at 16–13 Ma, supported by textures, mineral inclusions and trace elements. In the associated granulitized eclogites, zircon records only granulite/amphibolite facies overprinting at ~14 Ma, and titanite and rutile record cooling to 580–630 °C at 12.5–9 Ma. Granulite/amphibolite facies zircon has a low total REE relative to the protolith zircon, primarily due to the growth of REE-rich hornblende (total REE 80–260 μg/g), which removed 67–92% of the REE from the system. The low total REE of granulite/amphibolite facies zircon is comparable to the flat HREE reported for garnet-rich eclogite-facies zircon, and distinguishing these zircon types requires quantitative mineral volume estimates and other criteria. These findings may imply slower exhumation rates for some eclogite-facies terranes, such as the Tso Morari Himalaya and Papua New Guinea, than previously reported.

1. Introduction

High-pressure (HP) rocks formed in subduction/collision settings provide critical information for understanding plate tectonic processes. The exhumation rates of eclogites are most important in determining how tectonics accommodates plate velocities, which in turn influence exhumation mechanisms (Maruyama et al., 1996).

Petrochronological studies aim to constrain the timing of rock-forming processes and the rates of tectono-metamorphic or magmatic processes during orogenesis. Zircon petrochronology is widely used to obtain the ages of metamorphic stages (see Rubatto, 2017 and Kohn and Kelly, 2018 for a review). This approach requires that it can be demonstrated whether metamorphic zircon in high-pressure rocks grew during the eclogite-facies stage or cooling and/or after decompression (i.e., Kohn et al., 2015; Rubatto, 2017). Rubatto (2002) first proposed that eclogite-facies zircons are characterised by relatively flat heavy rare earth element (HREE) patterns and no Eu anomaly due to the presence of abundant garnet and the absence of plagioclase in the HP assemblage. Experimental studies and natural observations investigated the equilibrium partition coefficient between zircon and garnet in HP and high-temperature (HT) rocks (Hermann and Rubatto, 2003; Rubatto and Hermann, 2007; Taylor et al., 2015), which agree that a relatively flat HREE pattern in zircon indicates zircon growth in a garnet-rich assemblage, typical of high-grade rocks of appropriate bulk composition. This strategy has been applied to various rock types, suggesting that exhumation of HP rocks is fast and can proceed at plate tectonic velocities (e.

* Corresponding author.
E-mail address: wangjiamin@mail.iggcas.ac.cn (J.-M. Wang).

https://doi.org/10.1016/j.epsl.2024.119084
Received 14 May 2024; Received in revised form 10 October 2024; Accepted 15 October 2024
Available online 19 October 2024

g., Baldwin et al., 2004; Parrish et al., 2006; Rubatto et al., 2011; Gordon et al., 2012). However, Rubatto (2017) cautions that such a criterion should not be used indiscriminately to interpret zircon in eclogites and requires proper assemblage and equilibrium conditions. Studies have questioned this signature in eclogite-facies zircon that recrystallised and underwent partial to total resetting of their U–Pb system during the subsequent exhumation, whereas the REE system mainly remained unmodified (e.g., Pitra et al., 2022).

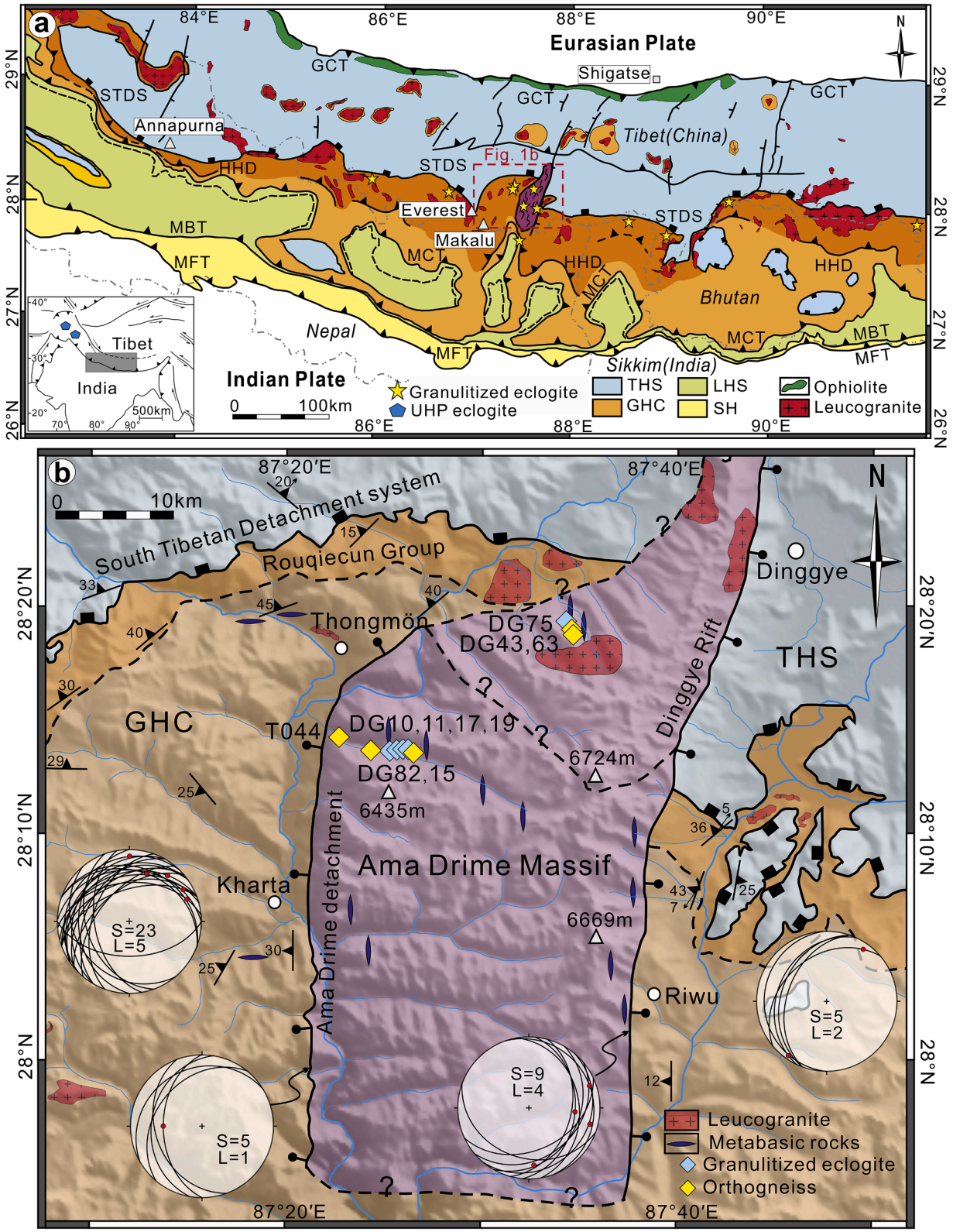

Fig. 1. Geological map of the central Himalaya (**a**) and Ama Drime Massif (**b**) (modified after Wang et al., 2021). GCT, Greater Counter Thrust; STDS, South Tibetan Detachment System; MCT, Main Central Thrust; MBT, Main Boundary Thrust; MFT, Main Frontier Thrust; HHD, High Himalayan Discontinuity. Projection: S, foliation; L, lineation.

Phase equilibrium modelling in Zr-bearing closed systems in high-temperature rocks with partial melting shows that metamorphic zircon should dissolve during prograde to peak conditions and primarily grow during cooling and melt crystallisation (Kelsey et al., 2008; Kelsey and Powell, 2011). This general trend also applies to open systems where melt loss is accounted for, which inhibits zircon increasing during cooling but still predicts limited zircon growth during prograde (Yakymchuk and Brown, 2014; Yakymchuk, 2023). Furthermore, mass-balance modelling suggests that omphacite- and garnet-forming reactions in eclogites consume Zr (Kohn et al., 2015) so that the above trend can be applied to HP mineral assemblages. The models assume equilibrium between all phases and zircon in contact with the melt/-fluid. They cannot account for zircon shielded from the melt/fluid or isolated melt patches not in equilibrium with the restite, which could occur in migmatites. Several studies have indeed argued for zircon growth during prograde metamorphism in eclogite- or granulite-facies rocks (e.g., Hermann and Rubatto 2003; Gauthiez-Putallaz et al. 2016; Johnson et al. 2021). In summary, modelling, experiments and studies of natural samples generally indicate that most zircon should grow mainly during exhumation and cooling after peak conditions and that a zircon growing in a garnet-bearing assemblage, independently if at peak-*P*, peak-*T* or decompression, should acquire a relatively flat HREE pattern.

In this study, we add insight into the significance of zircon REE patterns and show that a low total REE in zircon can be accounted for by the growth of REE-rich hornblende during granulite/amphibolite facies overprinting of HP rocks. Zircon, titanite, monazite and rutile petrochronology, thermodynamic modelling, trace element content of various rock-forming minerals, and compilation of the regional cooling histories of granulitized eclogites in the central Himalaya were used to support the petrogenesis of low total REE in zircon. The results provide an alternative setting for the production of flat HREE trace element patterns in zircon. The interpretation of dates in zircon requires more careful differentiation of hornblende-rich or garnet-rich eclogites and may infer slower exhumation rates of <10 mm/yr for eclogites that previously reported faster exhumation rates.

2. Geological setting

The Himalayan orogen is commonly divided into the Tethyan Himalayan Sequence, the Greater Himalayan Crystalline complex (GHC), the Lesser Himalayan Sequence (LHS) and the Sub-Himalayan Sequence (Fig. 1a), which are separated from north to south by the South Tibetan Detachment System (STDS), the Main Central Thrust, the Main Boundary Thrust and the Main Frontier Thrust (Fig. 1a, Yin, 2006). The GHC and LHS represent the Himalayan metamorphic core and have been intensively studied. The GHC consists mainly of amphibolite to granulite facies metasedimentary rocks and orthogneiss intruded by Oligocene–Miocene leucogranites (Yin, 2006). Granulitized eclogites are exposed as mafic lenses or pods within the metasedimentary rocks (Li et al., 2019; Wang et al., 2021). The LHS consists of Paleoproterozoic clastic deposits metamorphosed from greenschist facies to lower-amphibole facies and were formed by duplex structures with multiple imbricate thrusts.

The Ama Drime Massif (ADM) is located in the central part of the Himalayan orogenic belt (Fig. 1b). Structurally, the ADM represents an east-west extensional domal structure with its western wing (Ama Drime detachment) dipping eastward at 30°–60° (Kali et al., 2010), while its eastern wing (Dinggye Rift) offsets the STDS and dips eastward at 30°–50° with down-dip lineation (Zhang and Guo, 2007). The ADM is mainly composed of Paleoproterozoic orthogneisses (~1.8 Ga, Cottle et al., 2009) with an LHS affinity that has been metamorphosed to eclogite- and granulite-facies during the Himalayan orogeny. Abundant granulitized eclogite lenses are hosted by the orthogneisses (Lombardo and Rolfo, 2000; Groppo et al., 2007).

3. Sample description and petrography

Five mafic samples collected from the core (samples 16WDG10 and 16WDG11), mantle (sample 16WDG17) and rim (samples 16WDG19 and 16WDG75) portions of granulitized eclogite lenses within the ADM were studied along with orthogneiss directly in contact with the granulitized eclogites (samples 15DG82, 16WDG15, 16WDG43, 16WDG63 and T044) (Fig. 1b). Mineral abbreviations follow Warr (2021). Analytical methods and mineral compositions are reported in Appendix A or shown in Figs. S1 and S2.

3.1. Granulitized eclogite

The granulitized eclogite lenses can be as large as >50 m in diameter (Fig. 2a). Vertical two-mica leucogranite veins cut some granulitized eclogite lenses. Most of the granulitized eclogites are strongly overprinted, with increasing overprinting degrees toward the rim of the lens. Four main stages of mineral equilibration are recognized (Fig. 2b–f). The eclogite-facies stage (**M1**) is represented by omphacite, garnet mantle/rim and rutile; omphacite is preserved as inclusions in garnet mantle/rim with jadeite components as high as ~30% (Omp_1, Fig. S2a,b). Some prograde amphibole relicts are present as inclusions in the garnet core. A high-pressure granulite-facies stage (**M2**) is represented by Cpx_2+Pl_2 symplectites that were formed by replacement of omphacite (Fig. 2b,c), indicating ***Reaction I:*** Omp + Qz = Cpx + Pl (Groppo et al., 2007) or ***Reaction II:*** Grt + Omp + Rt = Cpx + Pl + Ilm (Cruciani et al., 2012). Rutile is locally replaced by ilmenite, and Bt_2+Pl_2 symplectites (Fig. 2c) are probably formed by the breakdown of phengite by ***Reaction III***: Phe + Qz = Bt +Pl (Groppo et al., 2007) or ***Reaction IV:*** Phe + Omp + Qz = Bt + Pl + Na-Cpx (Liu et al., 2023). A high- to ultra-high-temperature granulite-facies stage (**M3**) is represented by the mineral assemblage orthopyroxene, clinopyroxene, plagioclase, ±garnet, ilmenite/magnetite and titanite. Opx_3+Pl_3 symplectites developed at the rim of garnet (Fig. 2d) or clinopyroxene through the ***Reaction V:*** Grt + Omp/Cpx + Pl = Opx + Pl. The final re-equilibrated stage (**M4**) is represented by Hbl_4+Pl_4 symplectites formed by the breakdown of garnet rims or orthopyroxene (Fig. 2e) through ***Reaction VI:*** Grt + Pl + H_2O = Hbl + Pl (Cruciani et al., 2012). Note that ***Reactions I-VI*** are simplified versions of continuous reactions. The hornblende bands or grains are mainly within the symplectites forming lamellar intergrowths of Cpx_4+Pl_4+Hbl_4 symplectites (Fig. 2b), suggesting ***Reaction VII***: Omp/Na-Cpx + Qz + H_2O = Ca-Cpx + Pl + Hbl (Anderson and Moecher, 2007). The occurrence of ilmenite or magnetite varies in different samples depending on the Fe_2O_3 in the bulk system, but titanite is present as a retrograde phase in every sample collected. Zircon grains were observed in the Hbl_4+Pl_4 symplectites (Fig. 2f).

X-ray mapping by TIMA (TESCAN Integrated Mineral Analyzer) of samples collected from the same eclogite lens shows different mineral modal proportions. **1)** The lens core (sample 16WDG11) contains primarily plagioclase (47.3 vol.%), clinopyroxene (17.3 vol.%), orthopyroxene (14.7 vol.%) and hornblende (11.1 vol.%), with minor biotite (2.7 vol.%) and garnet (1.7 vol.%) (Fig. 2g). The relict garnet porphyroblasts (M1) are surrounded by abundant Opx_3+Pl_3 symplectites (M3) (Fig. 2g). The pseudomorphic replacement of garnet porphyroblasts results in Opx_3+Pl_3 symplectites (M3) in the interior and hornblende bands (M4) in the exterior (Fig. 2g). **2)** The lens mantle (sample 16WDG17) contains plagioclase (35.0 vol.%), hornblende (21.1 vol.%), garnet (11.6 vol.%), clinopyroxene (9.7 vol.%), biotite (3.4 vol.%) and orthopyroxene (3.3 vol.%) (Fig. 2h). Relict garnet porphyroblasts (M1) are better preserved and commonly replaced by Pl_4 corona (M4), widely referred to as "kelyphite" (Cruciani et al., 2012). The hornblende bands are along the margin of the Pl_4 corona and Cpx_2+Pl_2 symplectites (M2). **3)** The lens rim (sample 16WDG19) mainly contains hornblende (41.3 vol.%), plagioclase (35.5 vol.%), quartz (10.6 vol.%) and reduced propositions of clinopyroxene (6.9 vol.%) garnet (2.2 vol.%) and orthopyroxene (1.3 vol.%) (Fig. 2i). Pl_4 "kelyphite" and Hbl_4 bands (M4) replace the garnet

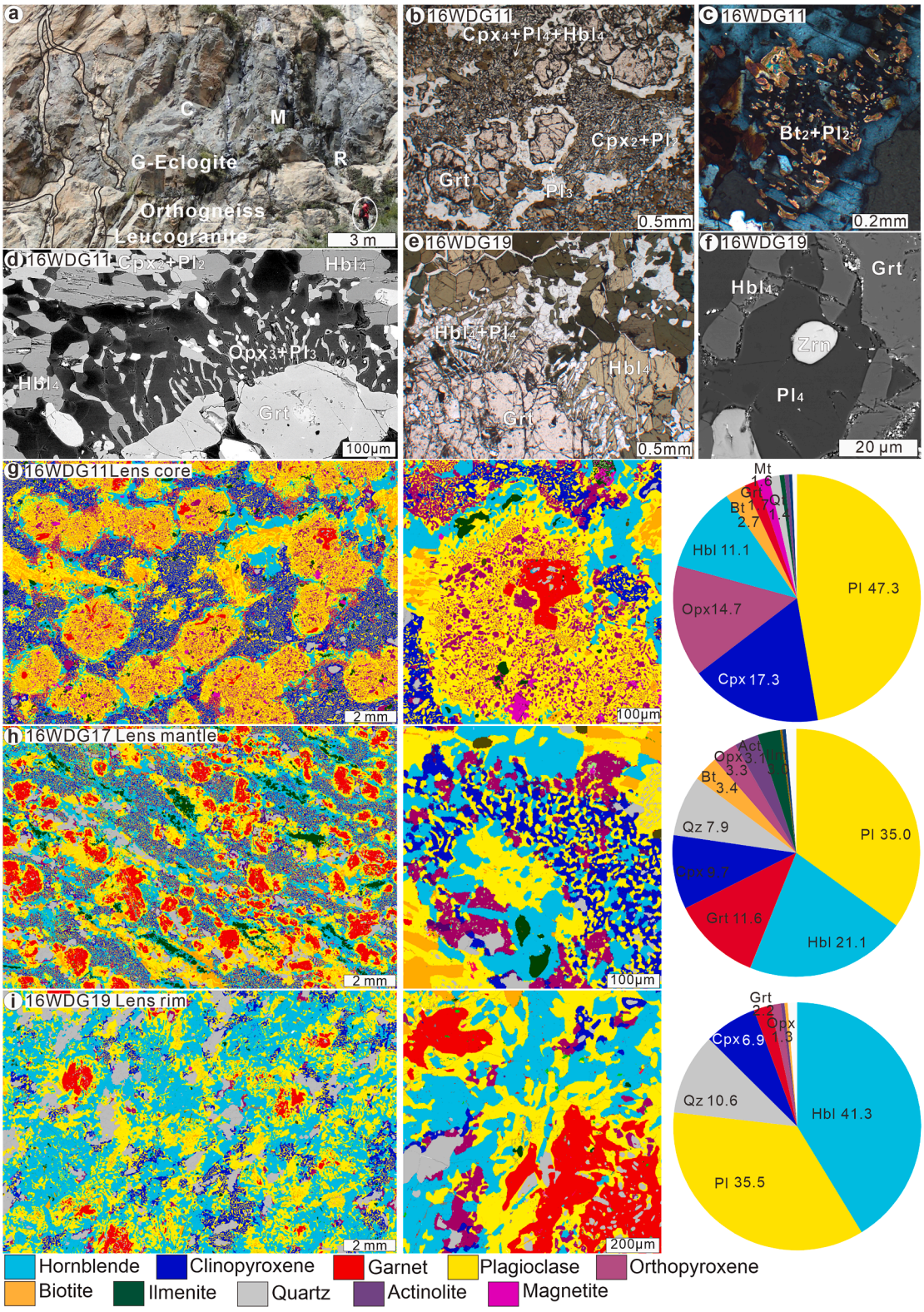

Fig. 2. Outcrop, photomicrographs and X-ray maps (warmer colour indicates higher intensity) of granulitized eclogites from the Ama Drime Massif. **a)** Granulitized eclogite embedded in migmatitic orthogneiss as a giant lens; **b)** Clinopyroxene + plagioclase symplectite from the breakdown of omphacite and garnet during retrogression; **c)** A biotite + plagioclase symplectite crystallises in local domains after phengite; **d)** Orthopyroxene + plagioclase symplectite as a corona of a relict garnet; **e)** Hornblende + plagioclase symplectite as a corona of a relict garnet, and large hornblende bands outside a symplectite; **f)** A zircon grain in the hornblende + plagioclase symplectite; **g–i)** TIMA X-ray mapping results of the granulitized eclogite in lens core, mantle and rim with decreasing abundance in clinopyroxene + plagioclase symplectites and orthopyroxene + plagioclase symplectites, but increasing abundance in hornblende. Mineral abbreviations are according to Warr (2021).

porphyroblasts and Cpx_2+Pl_2 symplectites (M2).

3.2. Orthogneiss

Most orthogneisses comprise biotite and feldspar + quartz bands, and typical minerals include biotite, plagioclase, K-feldspar, quartz, ± sillimanite, ± garnet, and ilmenite. K-feldspar often occurs as rotated porphyroblast, and biotite shows a mica fish structure.

4. Phase equilibrium modelling

Phase diagrams were calculated using GeoPS (Xiang and Connolly, 2022) and the internally consistent thermodynamic dataset of TC-DS622 (Holland and Powell, 2011) in the NCKFMASHTO system. The mineral activity-composition solutions (such as tonalitic melt, amphibole and augite from Green et al., 2016) are described in Appendix A. Granulitized eclogite samples 16WDG11 and 16WDG19 were used for phase equilibrium modelling. For each sample, XRF-based composition was used to estimate the *P-T* conditions. Theoretically, effective bulk composition (EBC) by subtracting the fractionated mineral proportions present at the M1-M2 stage (sodic-clinopyroxene, garnet core, rutile, phengite) should be used to estimate the *P–T* conditions of M3-M4 stage (Lanari and Engi, 2017). For simplicity, mineral fractionation was not considered in the models because volume proportions of omphacite,

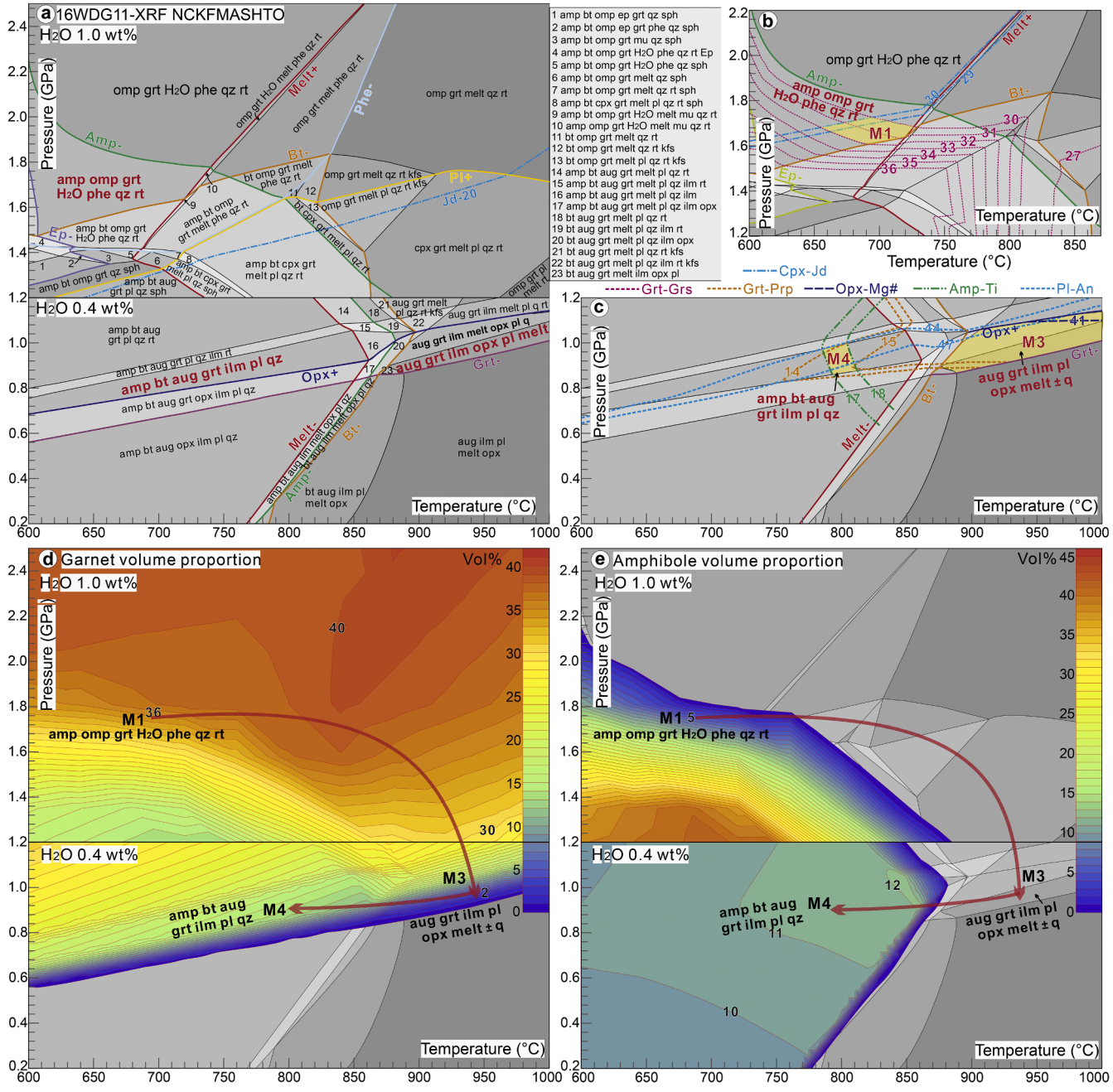

Fig. 3. Phase relationships, resulting pressure-temperature path (**a–c**) and garnet/amphibolite volume proportions (**d–e**) of granulitized eclogite sample 16WDG11. Phase diagrams were calculated using the XRF-measured bulk composition (wt%) of SiO_2(49.96), TiO_2(1.89), Al_2O_3(13.11), FeO(12.80), MgO(6.58), CaO(10.62), Na_2O(1.95), K_2O(0.70), O_2(0.191), H_2O(1.0 or 0.4) (NCKFMASHTO). Omphacitic pyroxene (Di) and augite (Aug) were used for labelling in the high-pressure field (>1.2 GPa) and medium- to low-pressure fields (<1.2 GPa), respectively, and the omphacitic pyroxene with a jadeite component larger than 20% was marked as omphacite (Omp).

rutile and phengite are rare (<1 vol%), and garnet compositions were strongly affected by diffusion during M3-M4 stage overprinting, preventing accurate fractionation at each stage. An H_2O component of 1.0 wt% was used to model dehydration reactions during prograde burial in the high-pressure range (1.2–2.5 GPa). H_2O components of 0.4 wt% and 0.85 wt% were used in the low-pressure range (0.2–1.2 GPa) for samples 16WDG11 and 16WDG19, respectively, which is the amount needed to grow the observed amphibole volume proportions (11.1 vol% and 41.3 vol%) during retrogression. T-H_2O diagrams at 1.0 GPa were also calculated to illustrate better the influence of H_2O on amphibole stability (Fig. S3).

4.1. Sample 16WDG11 (Lens core)

In the *P–T* phase diagram of sample 16WDG11 (Fig. 3a–e), the M1-stage mineral assemblage (Omp, Grt, Phe, Amp, Rt, Qz), the X_{Grs} in garnet mantle (0.3–0.32) and X_{Jd} of omphacite inclusions (~0.30) in garnet mantle were used to constrain the M1-stage *P-T* conditions at 660–720 °C and 1.60–1.80 GPa (geothermal gradient of 11–13 °C/km) (Fig. 3a,b). This is because garnet in the sample has been partly re-homogenized during granulite-facies overprinting, and the Fe and Mg compositions were likely reset. In contrast, the diffusion rate of Ca in garnet can be 1–2 orders of magnitude slower than Fe-Mg (Carlson, 2006). The observed M3-stage mineral assemblage (Aug, Grt, Ilm, melt, Opx, Pl, ±Qz) constrain the M3-stage *P-T* conditions at >880 °C and

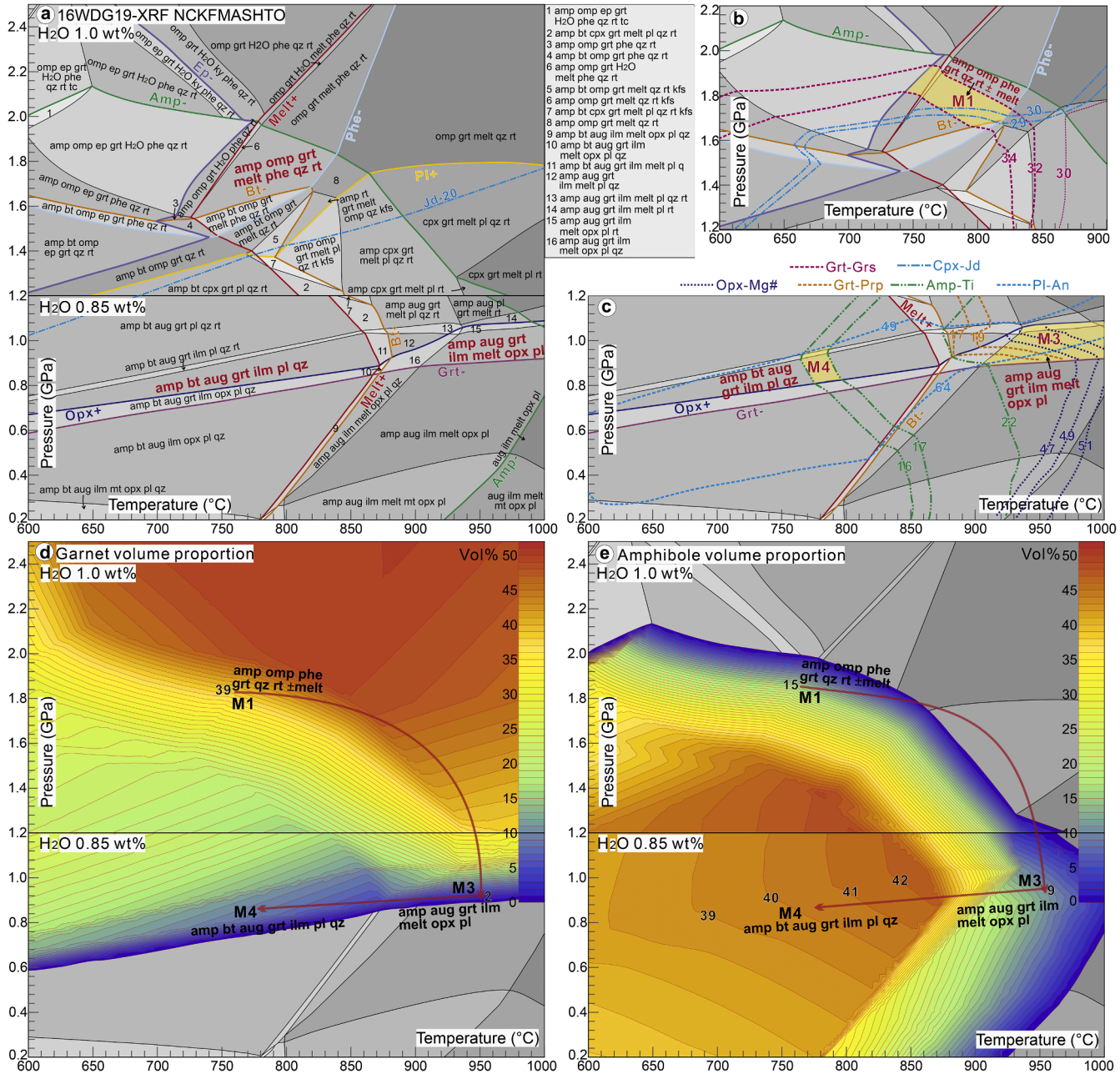

Fig. 4. Phase relationships, resulting pressure-temperature path (**a–c**) and garnet/amphibolite volume proportions (**d–e**) of granulitized eclogite sample 16WDG19. Phase diagrams were calculated using the XRF-measured bulk composition (wt%) of SiO_2(48.77), TiO_2(1.40), Al_2O_3(14.56), FeO(12.62), MgO(7.91), CaO(10.83), Na_2O(1.90), K_2O(0.50), O_2(0.322), H_2O(1.0 or 0.85) (NCKFMASHTO). Omphacitic pyroxene (Di) and augite (Aug) were used for labelling in the high-pressure field (>1.2 GPa) and medium- to low-pressure fields (<1.2 GPa), respectively, and the omphacitic pyroxene with a jadeite component larger than 20% was marked as omphacite (Omp).

0.8–1.1 GPa (Fig. 3a,c), where the highest Mg# in orthopyroxene (0.41) also intercept in this range, which is consistent with the Grt-Opx-Pl-Qz thermobarometer results (Fig. S4). The observed M4-stage mineral assemblage (Amp, Bt, Aug, Grt, Ilm, Pl, Qz), the highest X_{Prp} in garnet (0.14–0.15), average Ti contents (0.17–0.18) in hornblende, and plagioclase X_{An} values in the Hbl_4-Pl_4 symplectite (0.44–0.47) together constrain the M4-stage *P–T* conditions to 790–810 °C and 0.8–1.0 GPa (Fig. 3a,c). The results show a heating and decompression path from stage M1 to M3 and an isobaric cooling path from stage M3 to M4 (Fig. 3d,e).

4.2. *Sample 16WDG19 (Lens rim)*

In the *P–T* phase diagram of sample 16WDG19 (Fig. 4a–e), the M1-stage mineral assemblage (Omp, Grt, Phe, Amp, Rt, Qz, ±melt), the X_{Grs} in garnet core-mantle (0.32–0.34), and jadeite of omphacite inclusions (~0.30) constrain the M1-stage *P-T* conditions at 740–820 °C and 1.7–1.9 GPa (12–14 °C/km) (Fig. 4a,b). The M3-stage mineral assemblage (Aug, Grt, Opx, Pl, Ilm, melt, ±Amp), the X_{Prp} values in garnet (0.17–0.19), X_{An} values in plagioclase from the Opx_3-Pl_3 symplectite (0.64) and Mg# values in orthopyroxene constrain the M3-stage *P-T* conditions to be >900 °C and 0.9–1.0 GPa (Fig. 4a,c). The observed

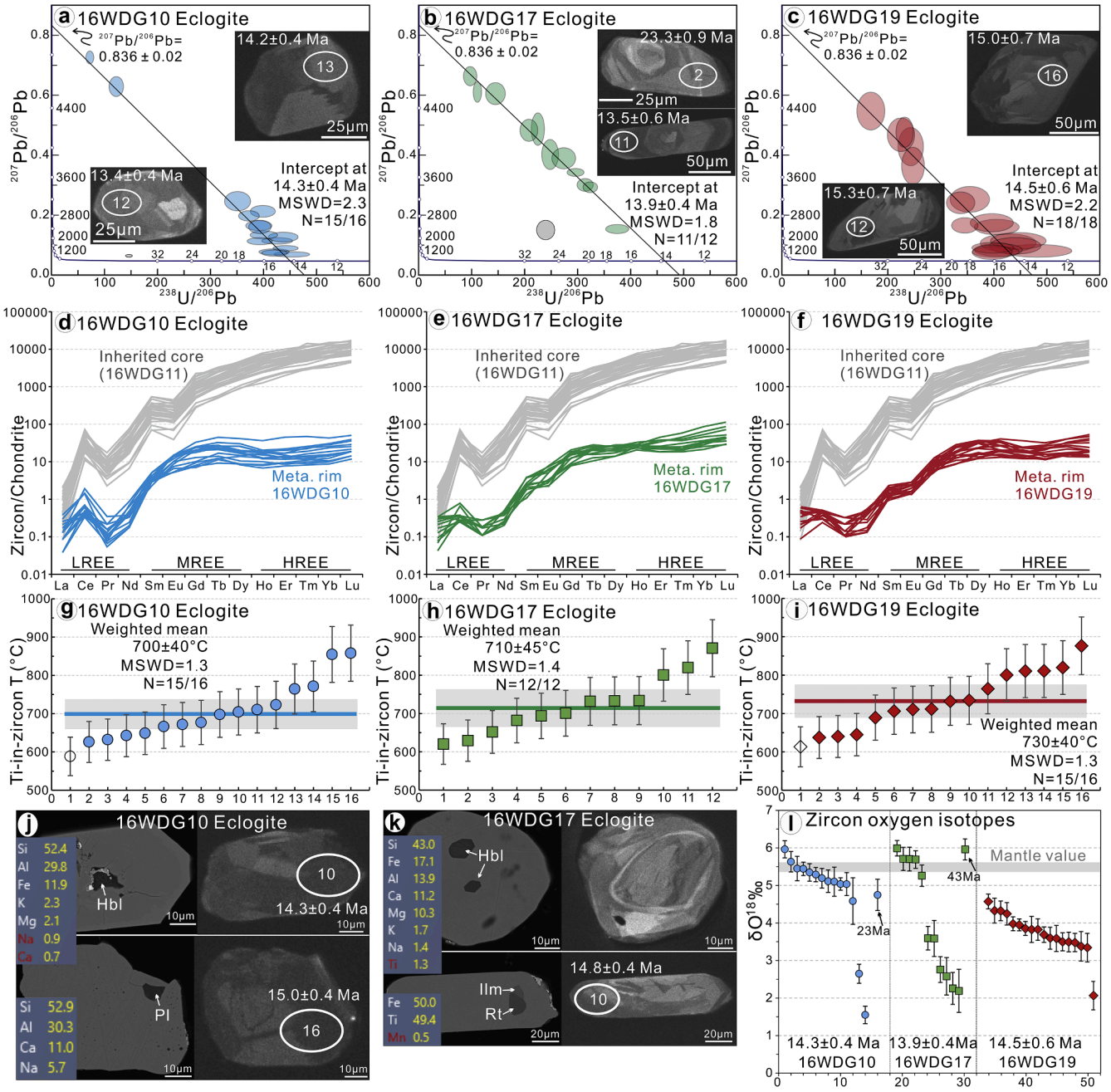

Fig. 5. Zircon textures, U-Pb ages, trace elements, mineral inclusions and oxygen isotopes from granulitized eclogites. **a–c**) Cathodoluminescence images and U-Pb ages of zircons; Mean zircon ages are $^{238}U/^{206}Pb$ ages; White cycles represent ion beam spots of ~25 μm; **d–f**) Chondrite-normalised (McDonough and Sun, 1995) trace element pattern of zircon from granulitized eclogites; Inherited cores are from sample 16WDG11 (Fig. S5); **g–i**) Temperatures calculated using titanium in zircon rims with the thermometer of Watson et al. (2006); **j,k**) Mineral inclusions in zircon from granulitized eclogites that were checked by EDS spectrometer with proportions of main elements; Left side are BSE images and right side are CL images of the same crystal; **l**) Zircon oxygen isotopic composition of granulitized eclogites.

M4-stage mineral assemblage (Hbl, Bt, Aug, Grt, Ilm, Pl, Qz, ±melt), average Ti content (0.16–0.17) and X_{An} values of plagioclase in the Hbl_4-Pl_4 symplectite (~0.49) constrain the M4-stage *P–T* conditions at 780–800 °C and 0.8–1.0 GPa (Fig. 4c). In summary, the results show a heating and decompression path from stage M1 to M3, and an isobaric cooling path from stage M3 to M4 (Fig. 4c).

4.3. Changes in mineral proportions along the inferred P–T paths

Along the constructed *P–T* paths, the volume fraction of garnet decreases from 35 to 40 vol% to ~2 vol% from M1 to M3 and remains low from M3 to M4 (Figs. 3d and 4d). Hornblende is consumed during prograde burial or heating, absent or nearly absent (0–10 vol%) at the M3 stage, but increases significantly from 0 to 11 vol% in sample 16WDG11 or from 9 vol% to 41 vol% in sample 16WDG19 from stage M3 to M4 (Figs. 3e and 4e). These estimates suggest that ~35 vol% of garnet could have been consumed during decompression heating from M1 to M3, and as much as ~32 vol% of hornblende could form during isobaric cooling from stage M3 to M4 in the studied samples.

5. U-Th-Pb petrochronology

5.1. Zircon in granulitized eclogites

All the zircon crystals analysed in this study were separated from granulitized eclogites. They are either texturally homogeneous or show a core-rim texture in cathodoluminescence (CL) (Fig. 5a–c). Some homogeneous grains or rims show sector/fir-tree zoning (Fig. 5a) or planar zoning (Fig. 5b,c). Most cores are bright and show weak oscillatory zoning (Fig. S5a). The U-Pb analyses show that the zircon rims contain common lead, and thus, the age is better calculated using a Tera-Wasserburg diagram plotting ratios uncorrected for common Pb. The regression of the analyses defines ages that are within uncertainty the same: 14.3 ± 0.4 Ma (2σ error, MSWD =2.3, sample 16WDG10), 13.8 ± 0.5 Ma (MSWD =1.8, sample 16WDG17), and 14.4 ± 0.6 Ma (MSWD =2.3, sample 16WDG19). The initial $^{207}Pb/^{206}Pb$ of the three samples are anchored at 0.836 ± 0.02 using the model common Pb for the age of 14 Ma, according to Stacey and Kramer (1975). The zircon cores of samples 16WDG10, 16WDG17 and 16WDG19 are too small (<25 μm) to be analysed by laser ablation. In sample 16WDG11, the zircon cores define a discordia line with an upper intercept age of 964 ± 15 Ma (MSWD =1.1), anchored by a group of concordant analyses (Fig. S5a).

In the chondrite-normalised diagram, the inherited cores have a pattern with a strong enrichment of HREE with respect to MREE and LREE (Lu_N/La_N 5100–46,000 and Lu_N/Gd_N 8.5–17.4), a negative Eu anomaly (Eu/Eu* 0.27–0.36) (Fig. 5d) and higher Th/U ratios (0.7–1.2). The rims have lower total REE contents than the inherited cores with relatively flatter patterns (Lu_N/La_N 30–400 and Lu_N/Gd_N 0.9–7.3), no to slightly negative Eu anomaly (Eu/Eu* 0.32–0.98) (Fig. 5d–f) and lower Th/U ratios (0.007–0.06). Most rims have titanium contents of 3–23 μg/g, and the calculated Ti-in-zircon temperatures using the thermometer of Watson et al. (2006) are in the 620–820 °C range. The weighted mean temperature estimates are 700 ± 40 °C (sample 16WDG10), 710 ± 45 °C (sample 16WDG17), and 730 ± 40 °C (sample 16WDG19).

Abundant hornblende, plagioclase, a few rutile and ilmenite were observed as inclusions in the zircon rims yielding Miocene ages (Fig. 5j, k). The zircon rims generally have low $\delta^{18}O$ values that cluster in two groups (Fig. 5l). Most zircon rims have $\delta^{18}O$ values of 4.7–6.0 ‰ (samples 16WDG10 and 16WDG17) or lower $\delta^{18}O$ values of 3.3–4.6 ‰ (sample 16WDG19). In each sample, a few analyses gave much lower $\delta^{18}O$ values of 1.5–3.0 ‰.

5.2. Titanite and rutile in granulitized eclogites

Titanite crystals in the analysed granulitized eclogites are generally homogeneous or sector-zoned in back-scattered electron (BSE) (Fig. S6a–d). Most grains have U contents of 20–400 μg/g, with a few up to ~755 μg/g. In all samples, the initial Pb fractions are high (40–85%), and therefore, lower intercept $^{238}U/^{206}Pb$ regression ages were obtained in the Tera-Wasserburg diagram plotting uncorrected ratios (Fig. S6a–d and Table S5): 12.5 ± 1.0 Ma (MWSD =3.1, sample 16WDG10), 10.0 ± 0.8 Ma (MWSD =0.3, sample 16WDG11), 11.2 ± 0.6 Ma (MWSD =0.5, sample 16WDG17), and 11.4 ± 0.7 Ma (MWSD =0.8, sample 16WDG19). The initial $^{207}Pb/^{206}Pb$ ratio for three samples is below the bulk Earth model value (0.588 ± 0.013, 0.705 ± 0.006, and 0.550 ± 0.015, respectively), indicating that the initial Pb had a radiogenic component.

Rutile crystals in the analysed granulitized eclogites do not show any internal zoning in BSE (Fig. S6e–h) and have U contents mostly between 20 and 60 μg/g. The rutile analyses have moderate or low proportion of initial Pb, and most analyses define concordia ages of 10.1 ± 1.2 Ma (MWSD =0.95, sample 16WDG10), 14.6 ± 0.6 Ma (MWSD =0.08, sample 16WDG11), 11.2 ± 0.6 Ma (MWSD =1.2, sample 16WDG17), and 9.0 ± 0.6 Ma (MWSD =0.01, sample 16WDG19).

5.3. Monazite in orthogneiss

Monazite crystals analysed in this study were separated from orthogneiss. They are generally homogeneous or have a core-rim structure in BSE images (Fig. 6a–e). For young monazites, excess ^{206}Pb due to decay of ^{230}Th can lead to overestimating the actual age (Schärer, 1984). Therefore, the $^{208}Pb/^{232}Th$ dates are preferred to the $^{206}Pb/^{238}U$ dates. For most analyses, the concordant degrees between $^{208}Pb/^{232}Th$ dates and $^{206}Pb/^{238}U$ dates are above 90%. In the garnet-free orthogneiss T044, 13 core analyses yield scattered $^{208}Pb/^{232}Th$ dates of 14.3–11.4 Ma, whereas the 19 rims have younger dates of 11.2–9.5 Ma (Fig. 6a). In other samples, the analyses return homogeneous group of $^{208}Pb/^{232}Th$ dates (Fig. 6b–d) with averages at 13.4 ± 0.1 Ma (MSWD =0.8, sample 15DG82), and 16.3 ± 0.1 Ma (MSWD =1.3, sample 16WDG63). In sample 16WDG43, 25 monazite dates scatter over a wide range of 16.0–14.8 Ma but largely overlap with the other samples. The monazite HREE and Y of these garnet-absent samples are available in Table S7. In the Grt-Bt-Sil orthogneiss 16WDG15 (Fig. 6e), monazite core analyses yield scattered $^{208}Pb/^{232}Th$ dates of 25.6–19.2 Ma (N = 12), which are not necessarily concordant with the $^{206}Pb/^{238}U$. The monazite rims yield younger dates of 18.8–16.5 Ma (N = 12). HREE and Y compositions increase from the cores to the rims with decreasing dates (Fig. 6f). Mineral inclusion in monazite are sillimanite, Bt+Kfs+Qz polyphase inclusions, apatite + xenotime + thorite polyphase inclusion, biotite, plagioclase and corundum (Fig. 6g–l).

6. Trace element composition of rock-forming minerals

The trace element composition of garnet, amphibole, clinopyroxene, orthopyroxene, biotite, plagioclase, titanite, and rutile in granulitized eclogites was analysed to quantify changes in the REE distribution in minerals during metamorphism. The results show that zircon cores have the highest total REE, HREE and MREE, whereas rims have much lower REE contents (Fig. 7a,b). Zircon rims have Th/U ratios of 0.001–0.1, while all the metamorphic minerals except rutile have higher Th/U ratios mostly within 0.1–10 (Fig. 7c). Titanite is enriched in LREE, Th and U and slightly depleted in HREE (Fig. 7a–c). Amphiboles in different textural positions (Hbl_4 matrix, Hbl_4-Pl_4 symplectite and inclusions in garnet) have identical REE contents, with a high total REE, a flat pattern and slightly negative Eu anomaly (Fig. 7a,b,d). Compared to hornblende, garnet has a similar high HREE content but is depleted in LREE and MREE, with no difference between large and small grains (Fig. S7g–h). Clinopyroxene in the symplectites has a flat pattern and slightly negative Eu anomaly, whereas omphacite inclusions have a slightly higher LREE, lower HREE and no Eu anomaly (Fig. 7a,b,d). Orthopyroxene is significantly lower in REE, with a left-leaning pattern enriched in HREE. Biotite has the lowest REE content, and elements such

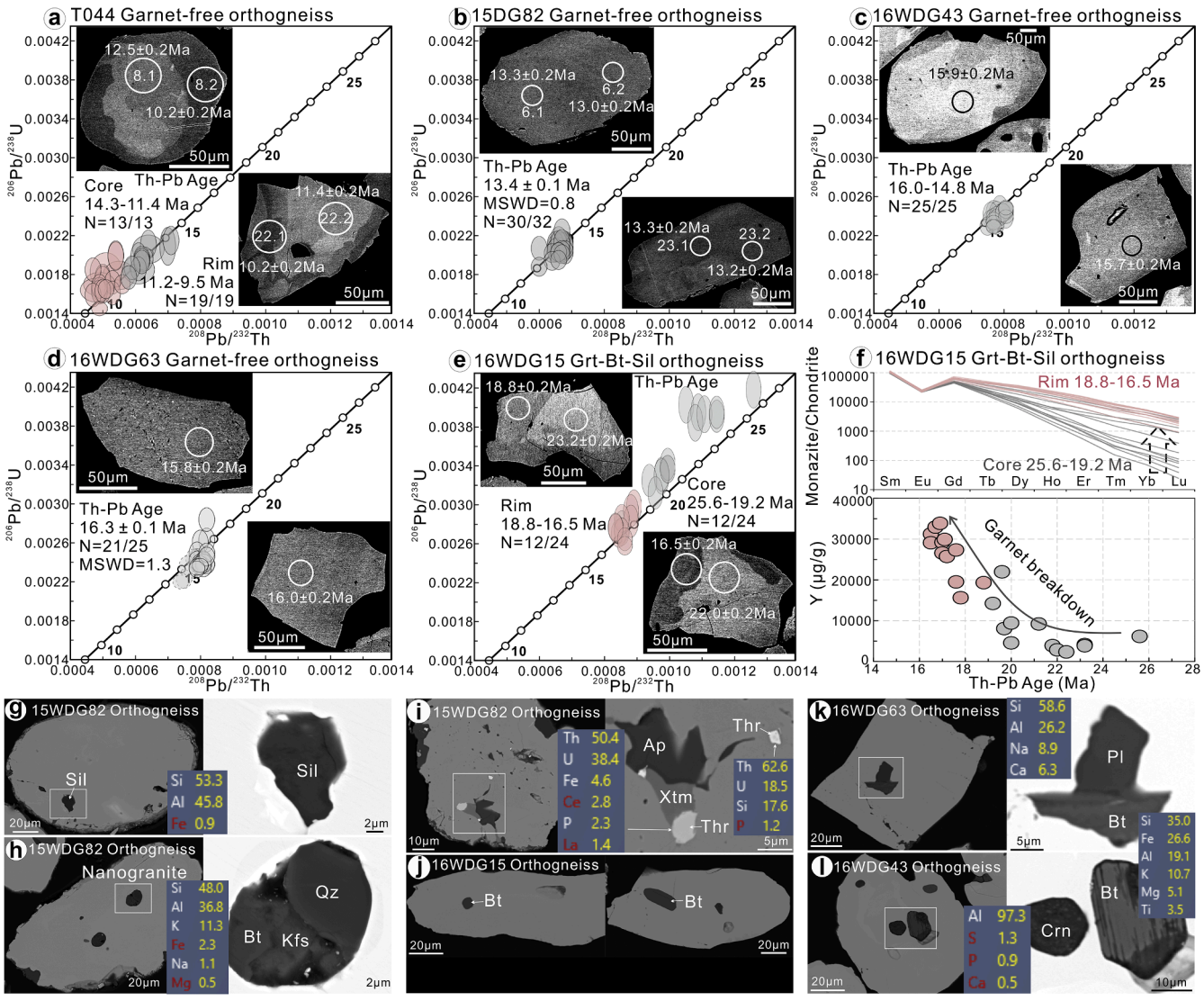

Fig. 6. Monazite textures, U-Th-Pb ages, trace elements and mineral inclusions from studied orthogneiss. **a–e**) Monazite U-Th-Pb age plots and BSE images showing textures; White cycles represent laser beam spots of ~24 μm; **f**) Chondrite-normalised (McDonough and Sun, 1995) REE patterns and Y contents versus dates of monazite from orthogneiss sample 16WDG15; **g–l**) Mineral inclusions in the monazite from orthogneiss that were checked by EDS spectrometer with proportions of major elements.

as Eu are close to the detection limit. Plagioclase is REE poor, with a mild enrichment in LREE and a strong positive Eu anomaly.

A mass balance calculation of trace element distribution in minerals was done by considering the modal proportions (weight%) calculated using the measured volume proportions (Table S1) and density of compositional end-members (Table S9) with the method of Zack et al. (2002). Percentages of the mineral end-members were calculated using the measured average compositions of minerals in Tables S2 and S3. The volume proportions of main rock-forming minerals, as well as accessory minerals like zircon (0.01–0.03 vol%), titanite (~0.02 vol%), and rutile (~0.01 vol%), were obtained by TIMA X-ray mapping using a resolution of ~3 μm, that generally give good modal estimates (Table S1). Abundances of zircon and rutile may bear significant uncertainties due to their tiny sizes in thin sections (10–30 μm), but it will not influence the distribution ratios of REE among hornblende, garnet, clinopyroxene and plagioclase, whose volumes are more robust. The volume proportions of amphibole and omphacite inclusions in garnet were too low (<1 vol%) to be considered. Despite its low proportion, the results show that Zr is mainly hosted by zircons (83–96 %, Fig. 7f–h). Titanium is mainly hosted by hornblende (44–89 %) or biotite (4–41 %), whereas titanite-bearing minerals like titanite and rutile contribute much less due to their low volume proportions (0.01–0.02 vol%). Europium is mainly hosted by hornblende and plagioclase. In all the samples, total REE, LREE, MREE and HREE are dominantly hosted by hornblende (53–92 %, Fig. 7f–h), especially in samples with higher abundances of hornblende. In sample 16WDG17, garnet hosts ~34% of HREE, but hornblende hosts more HREE (~53%) due to its higher modal abundance.

7. Discussion

7.1. *P–T* evolution of the central Himalayan eclogites

Recovering the *P–T* evolution of eclogites is fundamental to the accurate interpretation of U-Th-Pb ages and for understanding the growth behaviour of zircon, which can be challenging due to strong overprinting and non-equilibrated textures (Cruciani et al., 2012; Wang et al., 2021). For the central Himalayan eclogites, two types of *P–T* paths have been reported, which differ mainly for the M3 stage conditions but are relatively similar for the conditions of the M1 or M4 stage. The *P–T*

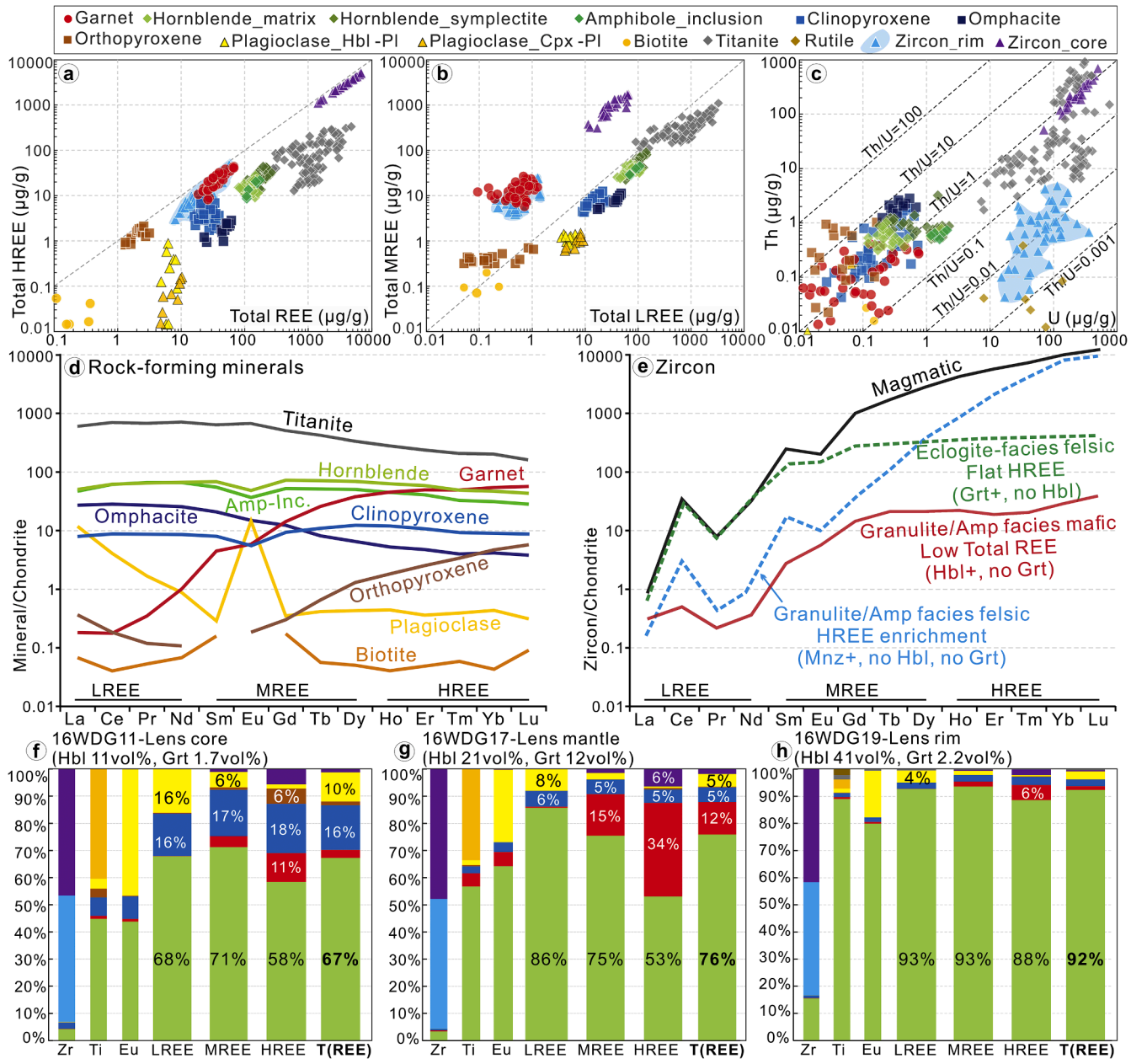

Fig. 7. Trace elements in rock-forming minerals and zircon from studied granulitized eclogites. **a,b**) Plots of total REE, HREE, MREE and LREE; **c**) Plot of Th versus U contents; **d**) Chondrite-normalised rare earth element patterns of rock-forming minerals; **e**) Chondrite-normalised rare earth element patterns of zircon; eclogite-facies zircon is from Rubatto (2002) and amphibolite-facies felsic zircon is from Rubatto (2017). Chondrite values are from McDonough and Sun (1995); **f–h**) Proportions of trace elements in rock-forming minerals and zircon from granulitized eclogites from the lens core, mantle and rim.

paths in earlier studies show a general trend of near isothermal decompression from eclogite facies of 2.0–2.1 GPa and 720–760 °C (M1) to granulite facies of 0.8–1.0 GPa and >750 °C (M2-M3), followed by isobaric cooling to amphibolite facies below 700 °C (M4) (Groppo et al., 2007; Wang et al., 2017). Recent studies from Mount Everest and Yadong have highlighted UHT conditions of 0.6–1.1 GPa and 900–970 °C for the temperature peak (M3) (Wang et al., 2021; Wu et al., 2022; Zhang et al., 2024).

Phase equilibrium modelling in this study has confirmed that the eclogite-facies assemblage formed at 660–720 °C and 1.6–1.9 GPa (M1) and was overprinted under UHT conditions of >900 °C and 0.8–1.1 GPa (M3) followed by final partial re-equilibrium at 780–810 °C and 0.8–1.0 GPa (M4). The results provide a new record of a decompression heating path to HT/UHT conditions for the central Himalayan eclogites, with a temperature increase of 180–240 °C during exhumation. Along the inferred *P–T* path, the most significant change in mineral proportions is the resorption of up to ~35 vol% of garnet (Figs. 3d and 4d) and the growth of ~32 vol% hornblende during decompression heating and subsequent isobaric cooling from M1 to M4 (Figs. 3e and 4e). Peak-stage minerals such as garnet and omphacite were likely still present as metastable minerals at the M3 stage, possibly with their compositions modified by diffusion, and then transformed into hornblende from M3 to M4 when water entered the system. Nevertheless, this does not influence the final modal proportions of garnet and hornblende from M1 to M4.

Hornblende should have formed mainly during the M4 stage because its formation requires the addition of water (Kohn, 1999), and the UHT stage is usually relatively dry, limiting the modal proportion of hornblende. The amount of H_2O available for metamorphic reaction influences the amphibole stability during phase equilibrium modelling. The calculated *T*-H_2O diagrams (Fig. S3) at 1.0 GPa show that amphibole

is not predicted to be stable if H_2O is extremely low (<0.22 wt% or <0.13 wt%) and can only be predicted to be stable at ultra-high temperatures with >0.25 wt% H_2O (sample 16WDG19) or >0.92 wt% H_2O (sample 16WDG11).

7.2. Petrochronology

Accessory minerals such as zircon and monazite in high-pressure rocks can grow or recrystallise at different stages of the subduction-exhumation cycle so that the age of a zircon and monazite domain cannot simply be assumed to date the pressure or temperature peak of the rock but must be related to *P–T* conditions (Rubatto, 2017). In the central Himalaya, it is debated whether zircon in granulitized eclogites records the timing of granulite-facies overprinting (Kellet et al., 2014; Wang et al., 2021) or eclogite-facies metamorphism (Wang et al., 2017; Li et al., 2019). Zircon ages are interpreted here only after monazite, titanite and rutile ages and a thorough tectono-metamorphic reconstruction.

Monazite U-Th-Pb ages of 16–13 Ma record melt crystallisation at temperatures below the UHT peak, while the 26–19 Ma ages record HT-UHT overprinting: **i)** Some mineral inclusions observed in the late monazite (16–13 Ma) can only be stable during low pressure and high temperatures, such as sillimanite (Fig. 6g), corundum (Fig. 6l), Bt+Kfs+Qz polyphase inclusions with negative crystal shape (Fig. 6h), interpreted as nanogranite crystallising from a melt (Cesare et al., 2009), and polyphase inclusion of apatite + xenotime + thorite (Fig. 6i), which is typically seen in hydrothermal low-pressure conditions (Frondel and Collette, 1957). **ii)** In a closed system, garnet breakdown releases HREE and Y, which can then be redistributed to simultaneously growing monazite or xenotime at lower temperatures; instead, garnet growth consumes HREE and Y (Pyle et al., 2001; Kohn et al., 2004). Unlike the granulitized eclogites, the orthogneiss samples do not contain

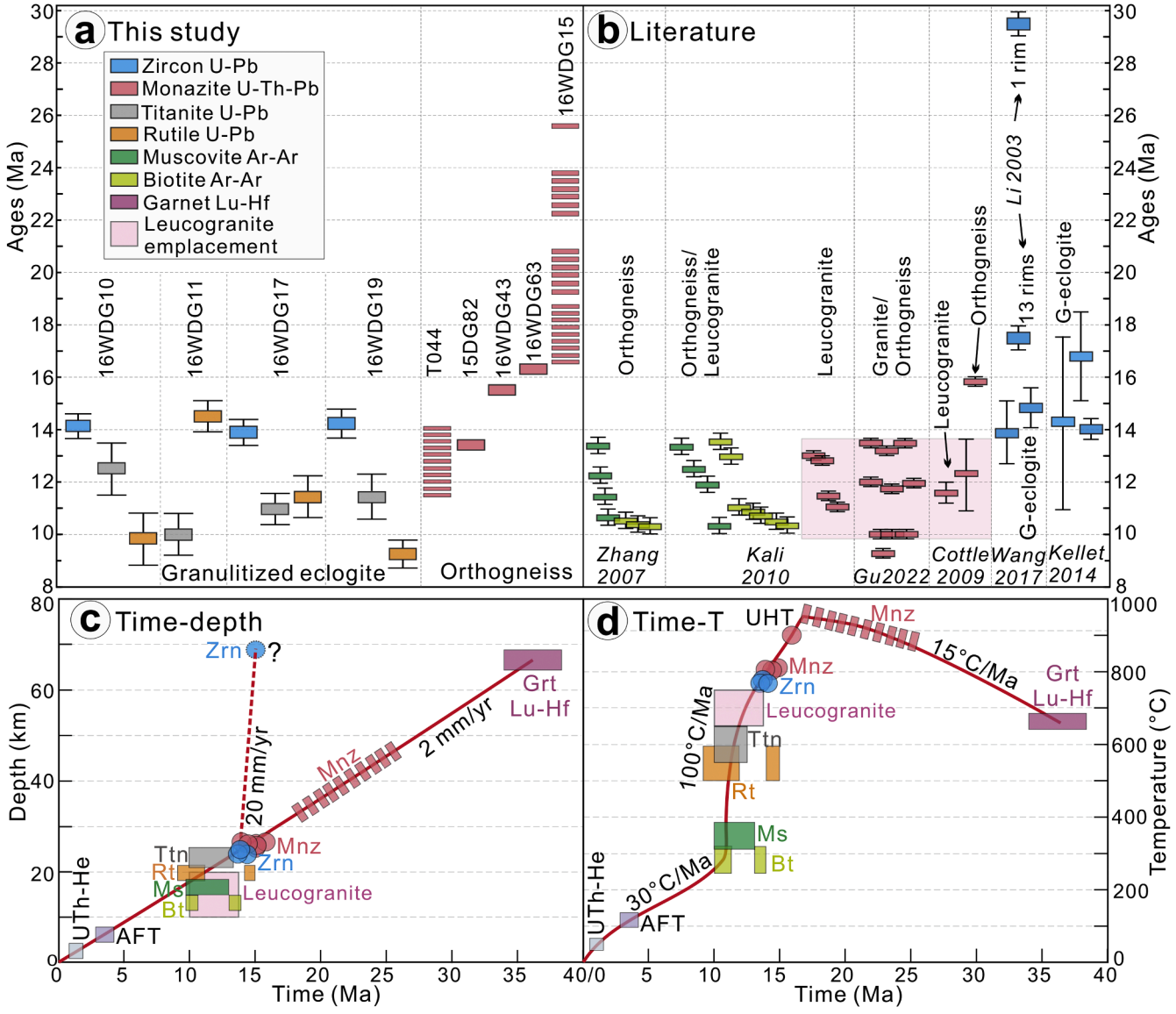

Fig. 8. Summary of isotopic ages and metamorphic timescale in the Ama Drime Massif. **a**) Summary of U-Th-Pb ages in granulitized eclogites and orthogneiss from this study; **b**) Summary of U-Th-Pb ages and Ar-Ar cooling ages in granulitized eclogites, orthogneiss and leucogranite in literature; Abbreviation of ages from previous studies: Li et al., 2003; Zhang and Guo, 2007; Cottle et al., 2009; Kali et al., 2010; Kellet et al., 2014; Wang et al., 2017; Gu et al., 2022; **c,d**) Reconstructed time-depth and time-temperature curves for the granulitized eclogites using U-Th-Pb ages of various minerals, mica Ar-Ar ages, apatite fission track and apatite U-Th-He ages; The exhumation rate of 20 mm/yr is according to Wang et al. (2017), while 2 mm/yr is from this study; depth and temperature information of zircon and monazite U-Th-Pb ages and garnet Lu-Hf ages are according to the obtained *P–T* path; The depth was calculated using pressure by assuming 0.333 km/GPa; temperature information of titanite and rutile U-Th-Pb ages are according to Pb volume diffusion.

hornblende or titanite, so garnet remains the main REE carrier. In the Grt-Bt-Sill orthogneiss sample 16WDG15, HREE and Y contents in monazite increase from the cores (25.6–19.2 Ma) to the rims (18.8–16.5 Ma), suggesting that the rims should record the time after garnet breakdown. The monazite cores should record resetting during HT-UHT overprinting rather than eclogite-facies as they have inclusions of biotite, which are not predicted to be stable at eclogite-facies in the models (Fig. 6j).

Titanite U-Pb ages 13–10 Ma are interpreted to record cooling under temperature conditions of ~600 °C. The closure temperature of the U–Pb system in accessory minerals depends mainly on grain radius and cooling rate, with larger crystals cooling faster and having higher closure temperatures. Experiments show that at cooling rates of 10 °C/Ma, comparable to those proposed for the Himalayan metamorphic core (Kali et al., 2010), the Pb-in-titanite closure temperature for a ~100 μm radius grain is ~600 °C (Cherniak, 2006). The peak metamorphic temperatures (>900 °C) are much higher than the Pb-in-titanite closure temperature, implying that titanite ages do not record the timing of peak metamorphism.

Rutile U-Pb ages 14–9 Ma are interpreted to record cooling at 580–630 °C. Pb volume diffusion experiments show that rutile with a radius of ~100 μm has a closure temperature of ~580 °C (cooling rate 1 °C/Ma, Cherniak, 2000). Considering that most rutile grains in our samples have a radius of ~50 μm and the ADM underwent a faster cooling (30–100 °C/Ma, Kali et al., 2010), a high closure temperature of 580–630 °C is used as the Pb-in-rutile closure temperature, which is much lower than the peak metamorphic temperatures (>900 °C). The age scatter (14–9 Ma) may be due to the large uncertainties of rutile U-Pb ages (± 1.5–4 Ma) and partial resetting of the U-Pb system in rutile during cooling across the sample, but the current data do not allow a more detailed analysis.

Timescale of metamorphism in the ADM: The above age interpretations are summarized along with published ages, providing a basis for unravelling the regional metamorphic timescale (Fig. 8). **I)** Eclogite-facies metamorphism (M1) probably occurred as early as 38–34 Ma, as indicated by garnet Lu-Hf dating of granulitized eclogites (Fig. 8c, d, Kellet et al., 2014); **ii)** Decompression heating (M1 to M3) occurred during 30–16 Ma as constrained by selected monazite U-Th-Pb ages in orthogneiss (Fig. 8a); **iii)** Isobaric cooling from peak-*T* to final partial re-equilibrium (M4) occurred during 16–13 Ma, as indicated by most monazite U-Th-Pb ages in orthogneiss and zircon U-Pb ages in granulitized eclogites (Fig. 8b); **iv)** Cooling to 650–500 °C occurred at 13–10 Ma, as constrained by titanite and rutile U-Pb ages, and leucogranite emplacement with depth of 15–10 km (Fig. 8a, Cottle et al., 2009; Gu et al., 2022); Cooling to 350–280 °C occurred at 11–10 Ma as recorded by mica Ar-Ar ages (Zhang and Guo, 2007; Kali et al., 2010); **v)** The reconstructed timescale of metamorphism and cooling suggests an average exhumation rate of ~2 mm/yr (Fig. 8c) and rapid cooling by ~100 °C/Ma after the peak-*T* (Fig. 8d).

7.3. Petrogenesis of zircon low total REE

After reconstructing the metamorphic timescale and combining all the following evidence, we conclude that the ~14 Ma zircon rims in the granulitized eclogites grew at granulite/amphibolite facies rather than eclogite-facies metamorphism based on the following points. **1)** The coexistence of low-pressure mineral inclusions of hornblende, plagioclase and ilmenite in zircon rims (Fig. 5g,h) represents the M4 stage mineral assemblage; this inclusion assemblage also excludes the possibility that the zircon U-Th-Pb systematics was reset at (U)HT conditions while preserving eclogite-facies REE patterns. **2)** The sector, fir-tree or planar zoning textures (Fig. 5a–c) also align with zircons crystallisation typically from an anatectic melt at HT conditions (Corfu et al., 2003; Kunz et al., 2018). **3)** Average Ti-in-zircon temperatures of 700–730 °C suggest that most zircon rims grew at amphibolite-facies conditions. A few rims yielding higher temperatures of 830–850 °C may have already grown at granulite-facies conditions. **4)** The $\delta^{18}O$ of zircon in samples 16WDG10 and 16WDG17 (5–6‰) are mostly around the mantle value of ~5.5 ‰, whereas those in sample 16WDG19 have lower values of 2–4.5 ‰. This suggests that the metamorphic zircons may have grown from an in-situ melt/fluid released from the granulitized eclogites (closed system) with a $\delta^{18}O$ of ~5.5 ‰ or lower, as the Proterozoic continental flood basalts in the same tectonic unit (Zhang et al., 2022). External melt/fluid released from the 1.85 Ga felsic orthogneiss or the subducted Indian felsic continent (open system) would have higher $\delta^{18}O$ of 8–9 ‰ (Imayama et al., 2023). Therefore, metamorphic zircon grew in a closed system, and its low total REE was caused by partitioning with rock-forming minerals in the granulitized eclogites. **5)** A decoupling of zircon *U*−Pb ages and REE patterns, as described on pelitic granulites that underwent long-lasting (20–60 Myr) (U)HT metamorphism in the Ivrea Zone (Kunz et al., 2018), is characterized by significant scatter in zircon dates (310–240 Ma) and trace element composition (e.g. Th/U 0.001−2.0); this is distinct from our case with concentrated ages at ~14 Ma, relatively homogenous REE and Th/U ratios (Th/U 0.001−0.1).

Previous studies suggested that the zircon U-Pb age of ~14 Ma is the time of eclogite-facies metamorphism, mainly based on the preservation of omphacite inclusions and flat HREE pattern in zircons (Wang et al., 2017; Li et al., 2019). However, caution should be exercised when using omphacite, garnet and rutile to indicate eclogite-facies metamorphism. This is because **i)** omphacite can be partly preserved in the matrix in retrogressed or granulitized eclogites (O'Brien, 1993; Li et al., 2019), and **ii)** for retrogressed or granulitized eclogites where matrix omphacite is not well preserved, omphacites was likely consumed at the granulite-facies by ***Reaction V*** or at amphibolite-facies by ***Reaction VII***. Therefore, zircon grown under granulite/amphibolite facies conditions can envelop relict omphacite, which does not necessarily indicate eclogite-facies metamorphism.

Below, we explore why the zircon rims that grew at granulite/amphibolite facies conditions in the granulitized eclogites have a low total REE pattern. **1)** Amphibole is enriched in most REE, with total REE content ~4 times higher than garnet and ~7 times higher than clinopyroxene (Fig. 7a,b,d). LREE enrichment is ~130 times, and MREE enrichment is ~3 times in amphibole with respect to garnet, while their HREE contents are similar. Orthopyroxene, plagioclase and biotite host less REE than garnet and amphibole. Therefore, the low total REE in metamorphic zircon could be explained by incorporating REE into hornblende (67–92%) due to its relatively high REE content (80–260 μg/g) and high volume fraction (11–41 vol%) (Fig. 7f–h). **2)** The low REE and flat HREE in metamorphic zircon may be secondarily contributed by relict garnet (2–12% total REE). For samples where garnet is still present due to limited overprinting, zircon that grows at granulite/amphibolite facies conditions could still grow in an environment where garnet still holds the HREE. **3)** The lack of a pronounced negative Eu anomaly is probably caused by the presence of hornblende and clinopyroxene, which balanced the effect of plagioclase growth.

In Fig. 9, we summarise the proposed behaviour of zircon in the granulitized eclogites. From prograde to eclogite-facies metamorphism (M1), prograde rims could grow by dissolution-recrystallisation of inherited cores aided by metamorphic fluids. Such zircon rims are generally narrow (<10 μm) and have flat HREE due to garnet growth (Rubatto, 2002, 2017). During granulite-facies overprinting (M2-M3), almost all prograde rims, along with partial inherited cores, are dissolved into the melt due to the high Zr solubility (Kelsey et al., 2008; Kelsey and Powell, 2011). Therefore, preserving prograde ages is difficult for granulitized eclogites undergoing significant melting at HT-UHT. At this stage, garnet was resorbed by ***Reaction V*** to release HREE into the melt/fluid. During isobaric cooling from M3 to M4, metamorphic zircon crystallised from the in-situ melt/fluid. The Zr was mostly provided by the dissolution of zircon cores in the melt/fluid. ***Reactions VI*** and ***VII*** formed hornblende by consuming metastable garnet and omphacite. The REE budget of the melt/fluid is dominated by hornblende so the metamorphic zircon has a low total REE pattern.

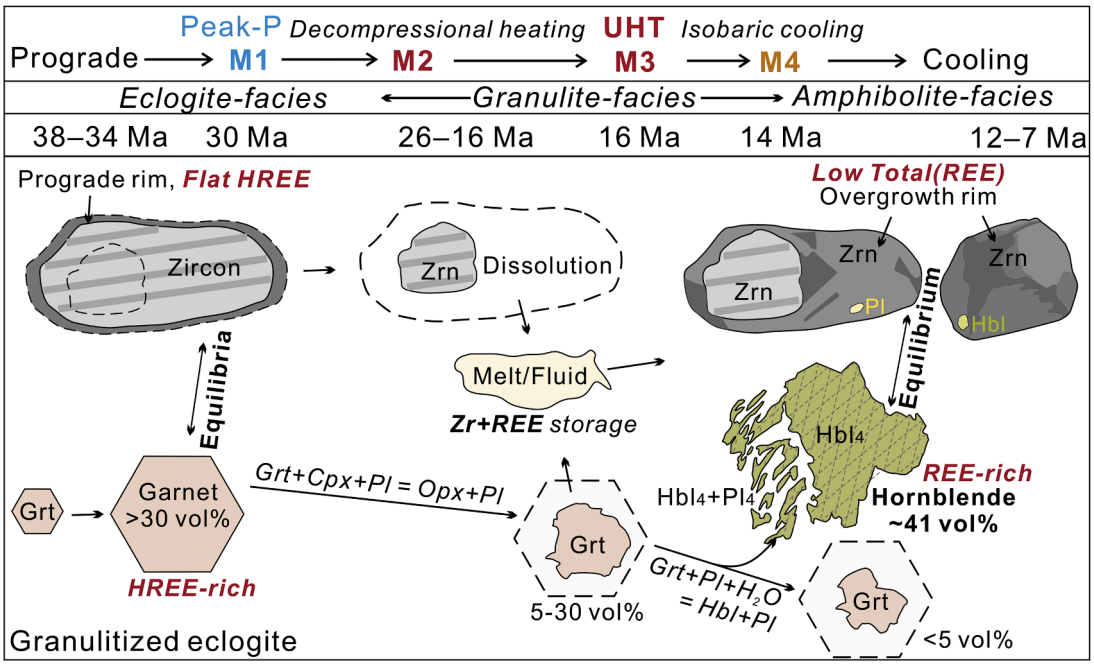

Fig. 9. Summary of the zircon and monazite behaviour in the granulitized eclogites and orthogneiss along the inferred *P–T* evolution of the Ama Drime Massif. The diagram also summarises the incorporation and release of REE in zircon due to the growth and breakdown of REE-rich garnet and hornblende along the whole *P–T* evolution (see text for discussion).

The low total REE in zircon is a remarkable feature that can be observed in metamorphic zircons from granulitized eclogites in ADM (Wang et al., 2017), Thongmon (Li et al., 2019; Wang et al., 2021), Bhutan (Grujic et al., 2011), and Indian Tso Morari (de Sigoyer et al., 2000; St-Onge et al., 2013). In other orogenic belts, such a feature is also commonly observed in metamorphic zircons from retrogressed or granulitized eclogites such as Papua New Guinea (Baldwin et al., 2004; Monteleone et al., 2007; Gordon et al., 2012), Variscan Bohemian Massif (Walczak et al., 2017), and Russian Kola Peninsula (Imayama et al., 2017). We argue that in samples with abundant amphibole, the low REE and flat HREE of metamorphic zircon is not necessarily diagnostic of eclogite facies but could also be amphibolite to granulite facies.

The flat HREE and absence of Eu anomaly in eclogite-facies zircon was first proposed by Rubatto (2002) by studying sub-solidus eclogitic micaschists, where their LREE and most MREE contents are relatively high and similar to magmatic zircon(green line versus black line in Fig. 7e). However, zircon with a low REE pattern reported in this study differs by a much lower total REE besides a similar flat HREE (red line in Fig. 7e). Such differences should be identified to avoid misinterpretation. Mafic rocks can be depleted in LREE compared to felsic rocks and are more likely to have metamorphic zircon with lower total REE, regardless of metamorphic grade. Particularly in mafic samples with abundant amphibole, a low total REE and flat HREE in zircon require further investigation considering aspects such as textures, mineral inclusions, oxygen isotopes, mineral abundances, and possibly dating of other minerals, before it can be interpreted as an eclogite-facies relict.

7.4. Implications to exhumation rates

Since zircon is widely used to date the timing of metamorphic stages in high-grade rocks, the petrogenesis of zircon with low total REE in retrogressed eclogites has broad implications on exhumation rates in worldwide orogenic belts. The exhumation rates vary by a factor of ~200 (from 0.5 mm/yr to ~100 mm/yr, Fig. 10a). This apparent variation across different orogenic belts or tectonic units could be due to different exhumation mechanisms. However, exhumation rates differing by a factor of as much as ~11 have been proposed even for eclogites from the same tectonic unit (Fig. 10b–d).

A first example is provided by the exhumation of central Himalayan eclogites. Based on our study and the reinterpretation of the low REE zircon, the timing of eclogitization in the ADM is proposed to be 38–34 Ma instead of ~14 Ma, which is ~20 Ma later than the initial collision (55–60 Ma, Leech et al., 2005). Consequently, the calculated linear exhumation rate is much slower at ~2 mm/yr instead of the proposed 20 mm/yr (Fig. 8c, Wang et al., 2017). These rocks remained in lower crustal conditions with high temperatures of 700–970 °C for >25 Ma instead of only ~2 Ma (Fig. 8c,d). The heat source for a prolonged (U)HT metamorphism was likely the combined effects of over-thickened radioactive felsic crust and asthenosphere upwelling (Wang et al., 2021; Zhang et al., 2024). A slow exhumation rate and long residence time at lower crustal conditions are in line with exhumation by steady-state underplating of high-grade metamorphic rocks to the orogenic crust (Wang et al., 2021).

For a second example, the timing of UHP metamorphism in the Tso Morari of western Himalaya is debated amongst 47–43 Ma (Donaldson et al., 2013), 50.8 ± 1.4 Ma (St-Onge et al., 2013) and 53.3 ± 0.7 Ma (felsic rocks, Leech et al., 2005) according to zircon U-Pb ages (Fig. 10b), yielding different exhumation rates of ~30, 8, or 6 mm/yr that differ by a factor of five (Fig. 10b). The interpretation of 47–43 Ma ages as UHP metamorphism is based on zircon flat HREE patterns and the absence of an Eu anomaly (Donaldson et al., 2013), but similar ages were also interpreted as continual crystallisation at amphibolite-facies conditions (Leech et al., 2005, 2007). Garnet Sm-Nd isochrons probably date cooling after the UHP metamorphism at 55 ± 7 Ma but with large uncertainties (de Sigoyer et al., 2000). Meanwhile, the timing of lower amphibolite-facies overprint (~600 °C, 1.0–1.2 GPa) is well constrained by phengite $^{40}Ar/^{39}Ar$ age of 48 ± 2 Ma (de Sigoyer et al., 2000), monazite Th-Pb age of 45.3 ± 1.1 Ma (St-Onge et al., 2013) and rutile U-Pb age of 44.1 ± 1.3 Ma (Wilke et al., 2010), supporting the interpretation of Leech et al. (2005, 2007). According to our new observation, the flat HREE and low total REE pattern recorded in the 47–43 Ma zircon (Fig. 10c) could be re-interpreted as partitioning growth with amphibole during retrogression as these eclogites were amphibolitized (36 vol% amphibole, St-Onge et al., 2013). This reassessment implies

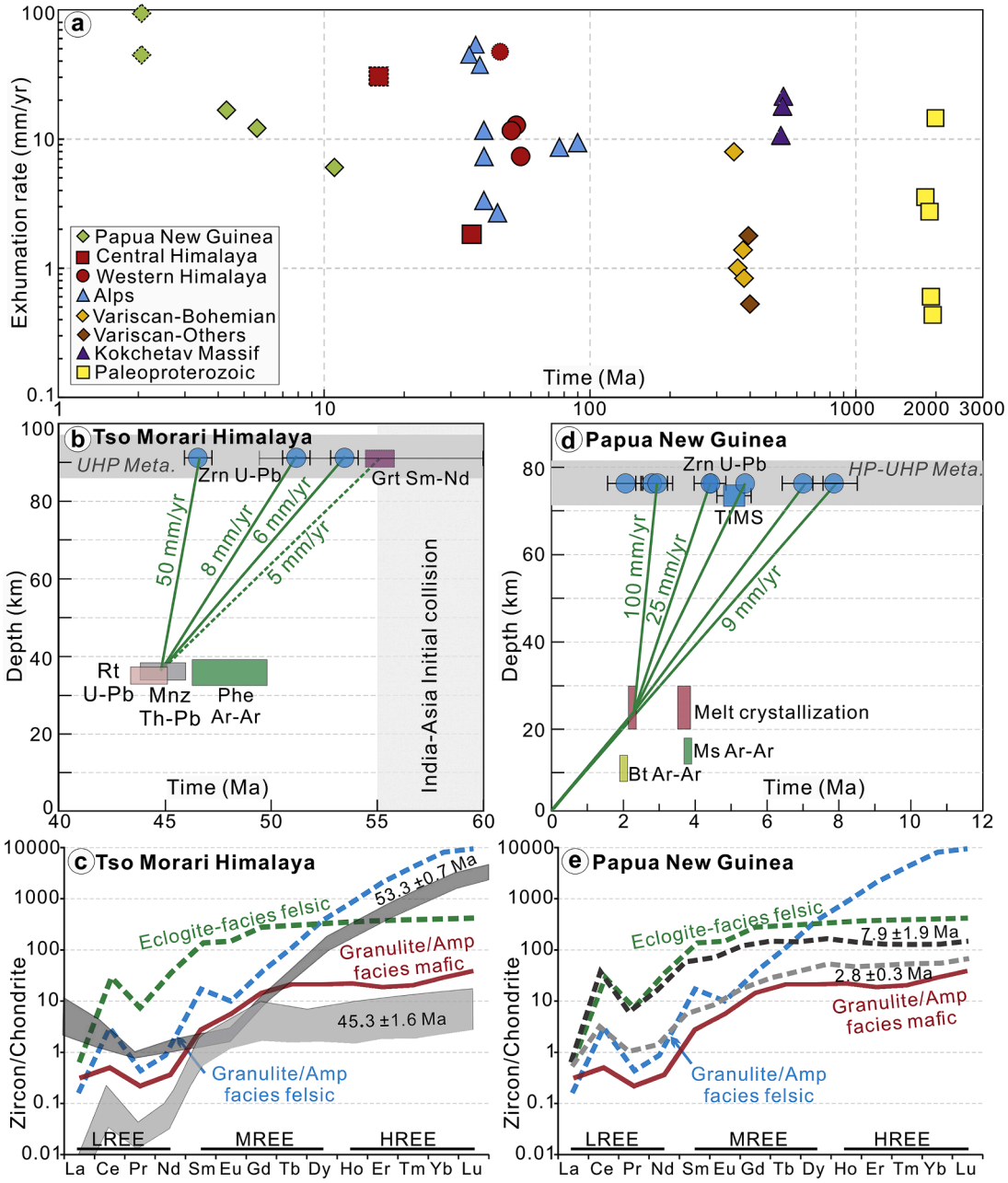

Fig. 10. Summary of zircon metamorphic ages and calculated exhumation rates in eclogites. **a)** Exhumation rates of representative eclogites worldwide through time since 2.0 Ga show the variation from 0.5 mm/yr to 100 mm/yr; References are attached in Appendix Table S10; Spots with dashed line are relatively fast exhumation rates calculated by zircon U-Pb ages interpreted as dating eclogite-facies metamorphism based on flat HREE patterns but could be re-interpreted as dating granulite/amphibolite facies metamorphism using the petrogenesis of low total REE from this study; **b,c)** Metamorphic ages, calculated exhumation rates and chondrite-normalised rare earth element patterns of metamorphic zircons in eclogites/gneiss from Tso Morari, western Himalaya; Zircon U-Pb ages, 45.3 ± 1.6 Ma (eclogite, Donaldson et al., 2013), 50.8 ± 1.4 Ma (eclogite, St-Onge et al., 2013) and 53.3 ± 0.7 Ma (gneiss without garnet, Leech et al., 2005); Garnet Sm-Nd isochrons: 55 ± 7 Ma (de Sigoyer et al., 2000); Phe $^{40}Ar/^{39}Ar$ age, 48 ± 2 Ma (de Sigoyer et al., 2000), phengite–apatite–rutile Rb–Sr age, 45.5 ± 4.4 Ma (de Sigoyer et al., 2000); Monazite Th-Pb age, 45.3 ± 1.1 Ma (St-Onge et al., 2013); Rutile U-Pb age, 44.1 ± 1.3 Ma (Wilke et al., 2010); **d,e)** Metamorphic ages, calculated exhumation rates and chondrite-normalised rare earth element patterns of metamorphic zircons in eclogites from Papua New Guinea; Zircon U-Pb ages of eclogites: SIMS age, 4.3 ± 0.4 Ma, Baldwin et al., 2004; ID-TIMS age 5.6–4.6 Ma, LA-ICP-MS age 9–4 Ma, Gordon et al., 2012; SIMS age, fresh eclogite 47.9 ± 1.9 Ma, amphibolitized eclogites 7.0 ± 1.0 Ma, 2.8 ± 0.3 Ma and 2.1 ± 0.5 Ma, Monteleone et al., 2007; Melt crystallisation, Gordon et al., 2012; Ar-Ar age, Baldwin et al., 1993.

that the Western Himalayan eclogites were probably exhumed at rates of 6–8 mm/yr rather than ~30 mm/yr.

A third example is the Papua New Guinea eclogites from Fergusson Island collected within an area of <30 km in diameter. Exhumation rates proposed for these eclogites vary by a factor of ~11 (from 9 mm/yr to ~100 mm/yr, Fig. 10d) due to different interpretations of zircon metamorphic ages as the timing of eclogite-facies metamorphism (4.3 ± 0.4 Ma, Baldwin et al., 2004; 5.6–4.6 Ma, Gordon et al., 2012; 7.9–2.1, Monteleone et al., 2007). The fresh eclogite yields a zircon age of 7.9 ± 1.9 Ma, whereas the amphibolitized eclogites yield ages of 7.0 ± 1.0 Ma, 2.8 ± 0.3 Ma and 2.1 ± 0.5 Ma, respectively, all of which were interpreted as dating diachronous UHP metamorphism (Monteleone et al., 2007). Some zircon grains in the Fergusson Island eclogites have a flat HREE pattern, but their low total REE resembles those in our study (Fig. 10e). According to our new interpretation, they may have formed during amphibolite facies overprinting as the amphibolitized eclogites

contain significant amounts of amphibole (>10 vol%, Monteleone et al., 2007; Gordon et al., 2012). Therefore, the exhumation rates of Papua New Guinea eclogites may need re-evaluation to determine whether they were exhumed at rates of <10 mm/yr or as fast as ~100 mm/yr.

8. Conclusions

1) The ADM granulitized eclogites underwent eclogite-facies metamorphism at 660–720 °C and 1.6–1.9 GPa (M1), were overprinted by high-pressure granulite-facies (M2) and then UHT metamorphism at >900 °C and 0.8–1.1 GPa (M3) and finally re-equilibrated at 780–810 °C and 0.8–1.0 GPa (M4). In the surrounding orthogneisses, monazite records resetting during HT-UHT overprinting at 26–19 Ma and melt crystallisation during cooling from peak-*T* at 16–13 Ma. Metamorphic zircon in the eclogites record granulite/amphibolite facies overprinting at ~14 Ma, while titanite and rutile record cooling to 580–630 °C at 12.5–9 Ma.
2) In the ADM granulitized eclogites, the granulite/amphibolite facies zircon has a low total REE pattern primarily due to the growth of REE-rich hornblende (80–260 μg/g), which can host 67–92% of the rock REE. The low total zircon REE pattern is similar but different from the flat HREE pattern interpreted as typical of eclogite-facies zircon. This finding calls for caution in interpreting zircon ages in amphibole-rich retrogressed eclogites as eclogite-facies or granulite/amphibolite facies based on a low REE content, with implications for exhumation rates.

CRediT authorship contribution statement

Jia-Min Wang: Writing – original draft, Methodology, Investigation, Funding acquisition, Conceptualization. **Daniela Rubatto:** Writing – review & editing, Methodology, Investigation, Conceptualization. **Pierre Lanari:** Writing – review & editing, Methodology, Investigation, Conceptualization. **Yu-Lu Tian:** Writing – review & editing, Investigation, Conceptualization. **Yi Chen:** Writing – review & editing, Investigation, Conceptualization. **Fu-Yuan Wu:** Writing – review & editing, Investigation, Conceptualization.

Declaration of competing interest

The authors declare that they have no known competing financial interests or personal relationships that could have appeared to influence the work reported in this paper.

Acknowledgements

We greatly appreciate the editorial handling by Prof. Alex Webb and constructive reviews by Dr. Chris Yakymchuk and an anonymous reviewer, which significantly improved the manuscript. J.M. Wang especially thanks Prof. Jin-Jiang Zhang for his long-term guidance and help in geology research. This work was supported by the National Key R&D Program of China (2022YFF0800800), the National Natural Science Foundation of China (42488201 and 42472074), the Second Tibetan Plateau Scientific Expedition and Research program (2019QZKK0703), the Institute of Geology and Geophysics Chinese Academy of Sciences (IGGCAS-202201), and the Youth Innovation Promotion Association of the Chinese Academy of Sciences (2022065).

Supplementary materials

Supplementary material associated with this article can be found, in the online version, at doi:10.1016/j.epsl.2024.119084.

Data availability

The data that has been used is confidential.

References

Anderson, E.D., Moecher, D.P., 2007. Omphacite breakdown reactions and relation to eclogite exhumation rates. Contrib. Mineral. Petrol. 154, 253–277.
Baldwin, S.L., Lister, G.S., Hill, E.J., Foster, D.A., McDougall, I., 1993. Thermochronologic constraints on the tectonic evolution of active metamorphic core complexes, D'entrecasteaux Islands. Papua New Guinea. Tectonics 12, 611–628.
Baldwin, S.L., Monteleone, B.D., Webb, L.E., Fitzgerald, P.G., Grove, M., June Hill, E., 2004. Pliocene eclogite exhumation at plate tectonic rates in eastern Papua New Guinea. Nature 431, 263.
Carlson, W.D., 2006. Rates of Fe, Mg, Mn, and Ca diffusion in garnet. American Mineralogist 91, 1–11.
Cesare, B., Ferrero, S., Salvioli-Mariani, E., Pedron, D., Cavallo, A., 2009. Nanogranite" and glassy inclusions: the anatectic melt in migmatites and granulites. Geology. 37, 627–630.
Cherniak, D.J., 2000. Pb diffusion in rutile. Contributions to Mineralogy and Petrology 139, 198–207.
Cherniak, D.J., 2006. Zr diffusion in titanite. Contributions to Mineralogy and Petrology 152, 639–647.
Corfu, F., Hanchar, J.M., Hoskin, P.W.O., Kinny, P., 2003. Atlas of Zircon Textures. Rev. Mineral. Geochem. 53, 469–500.
Cottle, J.M., Jessup, M.J., Newell, D.L., Horstwood, M.S.A., Noble, S.R., Parrish, R.R., Waters, D.J., Searle, M.P., 2009. Geochronology of granulitized eclogite from the Ama Drime Massif: implications for the tectonic evolution of the South Tibetan Himalaya. Tectonics. 28, TC1002.
Cruciani, G., Franceschelli, M., Groppo, C., Spano, M.E., 2012. Metamorphic evolution of non-equilibrated granulitized eclogite from Punta de li Tulchi (Variscan Sardinia) determined through texturally controlled thermodynamic modelling. J. Metamorph. Geol. 30, 667–685.
de Sigoyer, J., Chavagnac, V.r., Blichert-Toft, J., Villa, I.M., Luais, B.a., Guillot, S.p., Cosca, M., Mascle, G., 2000. Dating the Indian continental subduction and collisional thickening in the northwest Himalaya: multichronology of the Tso Morari eclogites. Geology. 28, 487–490.
Donaldson, D.G., Webb, A.A.G., Menold, C.A., Kylander-Clark, A.R.C., Hacker, B.R., 2013. Petrochronology of Himalayan ultrahigh-pressure eclogite. Geology. 41, 835–838.
Frondel, C., Collette, R.L., 1957. Hydrothermal Synthesis of Zircon, Thorite and Huttonite. American Mineralogist 42, 759–765.
Gauthiez-Putallaz, L., Rubatto, D., Hermann, J., 2016. Dating prograde fluid pulses during subduction by in situ U–Pb and oxygen isotope analysis. Contributions to Mineralogy and Petrology 171, 15.
Gordon, S.M., Little, T.A., Hacker, B.R., Bowring, S.A., Korchinski, M., Baldwin, S.L., Kylander-Clark, A.R.C., 2012. Multi-stage exhumation of young UHP–HP rocks: timescales of melt crystallization in the D'Entrecasteaux Islands, southeastern Papua New Guinea. Earth Planet. Sci. Lett. 351–352, 237–246.
Green, E.C.R., White, R.W., Diener, J.F.A., Powell, R., Holland, T.J.B., Palin, R.M., 2016. Activity–composition relations for the calculation of partial melting equilibria in metabasic rocks. J. Metamorph. Geol. 34, 845–869.
Groppo, C., Lombardo, B., Rolfo, F., Pertusati, P., 2007. Clockwise exhumation path of granulitized eclogites from the Ama Drime range (Eastern Himalayas). J. Metamorph. Geol. 25, 51–75.
Grujic, D., Warren, C.J., Wooden, J.L., 2011. Rapid synconvergent exhumation of Miocene-aged lower orogenic crust in the eastern Himalaya. Lithosphere 3, 346–366.
Gu, D., Zhang, J., Lin, C., Zheng, J., Feng, L., Fan, Y., Huang, B., 2022. Petrogenesis of monzonites and leucogranites in the Ama Drime Massif: implications for sources and differentiation of Himalayan leucogranites. J. Asian Earth. Sci. 237, 105372.
Hermann, J., Rubatto, D., 2003. Relating zircon and monazite domains to garnet growth zones: age and duration of granulite facies metamorphism in the Val Malenco lower crust. J. Metamorph. Geol. 21, 833–852.
Holland, T.J.B., Powell, R., 2011. An improved and extended internally consistent thermodynamic dataset for phases of petrological interest, involving a new equation of state for solids. J. Metamorph. Geol. 29, 333–383.
Imayama, T., Bose, N., Yi, K., Jeong, Y.-J., Horie, K., Takehara, M., Kawabata, R., 2023. Zircon U–Pb, Hf, and O isotopic Constraints On the Tectonic Affinity of the Basement of the Himalayan orogenic belt: Insights from Metasedimentary rocks, orthogneisses, and Leucogranites in Garhwal, NW India, 397. Precambrian Research, 107183.
Imayama, T., Oh, C.-W., Baltybaev, S.K., Park, C.-S., Yi, K., Jung, H., 2017. Paleoproterozoic high-pressure metamorphic history of the Salma eclogite on the Kola Peninsula. Russia. Lithosphere 9, 855–873.
Johnson, T., Yakymchuk, C., Brown, M., 2021. Crustal melting and suprasolidus phase equilibria: from first principles to the state-of-the-art. Earth. Sci. Rev. 221, 103778.
Kali, E., Leloup, P.H., Arnaud, N., Maheo, G., Liu, D.Y., Boutonnet, E., Van der Woerd, J., Liu, X.H., Jing, L.Z., Li, H.B., 2010. Exhumation history of the deepest central Himalayan rocks, Ama Drime range: key pressure-temperature-deformation-time constraints on orogenic models. Tectonics. 29, TC2014.
Kellett, D.A., Cottle, J.M., Smit, M., 2014. Eocene deep crust at Ama Drime, Tibet: early evolution of the Himalayan orogen. Lithosphere 6, 220–229.
Kelsey, D.E., Clark, C., Hand, M., 2008. Thermobarometric modelling of zircon and monazite growth in melt-bearing systems: examples using model metapelitic and metapsammitic granulites. J. Metamorph. Geol. 26, 199–212.
Kelsey, D.E., Powell, R., 2011. Progress in linking accessory mineral growth and breakdown to major mineral evolution in metamorphic rocks: a thermodynamic approach in the Na_2O-CaO-K_2O-FeO-MgO-Al_2O_3-SiO_2-H_2O-TiO_2-ZrO_2 system. J. Metamorph. Geol. 29, 151–166.
Kohn, M.J., 1999. Why most "dry" rocks should cool "wet". American Mineralogist 84, 570–580.

Kohn, M.J., Corrie, S.L., Markley, C., 2015. The fall and rise of metamorphic zircon. American Mineralogist 100, 897–908.
Kohn, M.J., Kelly, N.M., 2018. Petrology and geochronology of getamorphic zircon, Microstructural geochronology: Planetary records down to atom scale pp 35–61.
Kohn, M.J., Malloy, M.A., 2004. Formation of monazite via prograde metamorphic reactions among common silicates: implications for age determinations. Geochim. Cosmochim. Acta 68, 101–113.
Kunz, B.E., Regis, D., Engi, M., 2018. Zircon ages in granulite facies rocks: decoupling from geochemistry above 850 °C? Contributions to Mineralogy and Petrology 173, 1–21.
Lanari, P., Engi, M., 2017. Local bulk composition effects on metamorphic mineral assemblages. Rev. Mineral. Geochem. 83, 55–102.
Leech, M.L., Singh, S., Jain, A.K., 2007. Continuous metamorphic zircon growth and interpretation of U-Pb SHRIMP dating: an example from the western Himalaya. Int. Geol. Rev. 49 (4), 313–328.
Leech, M.L., Singh, S., Jain, A.K., Klemperer, S.L., Manickavasagam, R.M., 2005. The onset of India–Asia continental collision: early, steep subduction required by the timing of UHP metamorphism in the western Himalaya. Earth Planet. Sci. Lett. 234, 83–97.
Li, D., Liao, Q., Yuan, Y., Wan, Y., Liu, D., Zhang, X., Yi, S., Cao, S., Xie, D., 2003. SHRIMP U-Pb zircon geochronology of granulites at Rimana (Southern Tibet) in the central segment of Himalayan orogen. Chinese Science Bulletin 48, 2647–2650.
Li, Q., Zhang, L., Fu, B., Bader, T., Yu, H., 2019. Petrology and zircon U–Pb dating of well-preserved eclogites from the Thongmön area in central Himalaya and their tectonic implications. J. Metamorph. Geol. 37, 203–226.
Liu, S., Zhang, G., Zhang, L., Webb, A.A.G., 2023. Omphacite melting and the destruction of early high-pressure rock records. Journal of Geophysical Research: Solid Earth 128, e2023JB027395.
Lombardo, B., Rolfo, F., 2000. Two contrasting eclogite types in the Himalayas: implications for the Himalayan orogeny. J. Geodyn. 30, 37–60.
Maruyama, S., Liou, J.G., Terabayashi, M., 1996. Blueschists and Eclogites of the World and Their Exhumation. Int. Geol. Rev. 38, 485–594.
McDonough, W.F., Sun, S.S., 1995. The composition of the Earth. Chem. Geol. 120, 223–253.
Monteleone, B.D., Baldwin, S.L., Webb, L.E., Fitzgerald, P.G., Grove, M., Schmitt, A.K., 2007. Late Miocene–Pliocene eclogite facies metamorphism, D'Entrecasteaux Islands, SE Papua New Guinea. J. Metamorph. Geol. 25, 245–265.
O'Brien, P.J., 1993. Partially retrograded eclogites of the Münchberg Massif, Germany: records of a multi-stage Variscan uplift history in the Bohemian Massif. J. Metamorph. Geol. 11, 241–260.
Parrish, R.R., Gough, S.J., Searle, M.P., Waters, D.J., 2006. Plate velocity exhumation of ultrahigh-pressure eclogites in the Pakistan Himalaya. Geology. 34, 989–992.
Pitra, P., Poujol, M., Van Den Driessche, J., Bretagne, E., Lotout, C., Cogné, N., 2022. Late Variscan (315 Ma) subduction or deceptive zircon REE patterns and U–Pb dates from migmatite-hosted eclogites? (Montagne Noire, France). J. Metamorph. Geol. 40, 39–65.
Rubatto, D., 2002. Zircon trace element geochemistry: partitioning with garnet and the link between U–Pb ages and metamorphism. Chem. Geol. 184, 123–138.
Rubatto, D., 2017. Zircon: the metamorphic mineral. Rev. Mineral. Geochem. 83, 261–295.
Rubatto, D., Hermann, J., 2007. Zircon Behaviour in Deeply Subducted Rocks. Elements 3, 31–35.
Rubatto, D., Regis, D., Hermann, J., Boston, K., Engi, M., Beltrando, M., McAlpine, S.R.B., 2011. Yo-yo subduction recorded by accessory minerals in the Italian Western Alps. Nature Geosci 4, 338–342.
Pyle, J.M., Spear, F.S., Rudnick, R.L., McDonough, W.F., 2001. Monazite–xenotime–garnet equilibrium in metapelites and a new monazite–garnet thermometer. Journal of Petrology 42, 2083–2107.
Schärer, U., 1984. The effect of initial 230Th disequilibrium on young UPb ages: the Makalu case. Himalaya. Earth and Planetary Science Letters 67, 191–204.
St-Onge, M.R., Rayner, N., Palin, R.M., Searle, M.P., Waters, D.J., 2013. Integrated pressure-temperature-time constraints for the Tso Morari dome (Northwest India): implications for the burial and exhumation path of UHP units in the western Himalaya. J. Metamorph. Geol. 31, 469–504.
Stacey, J.S., Kramers, J.D., 1975. Approximation of terrestrial lead isotope evolution by a two-stage model. Earth Planet. Sci. Lett. 26, 207–221.
Taylor, R.J.M., Harley, S.L., Hinton, R.W., Elphick, S., Clark, C., Kelly, N.M., 2015. Experimental determination of REE partition coefficients between zircon, garnet and melt: a key to understanding high-T crustal processes. J. Metamorph. Geol. 33, 231–248.
Walczak, K., Anczkiewicz, R., Szczepański, J., Rubatto, D., Košler, J., 2017. Combined Garnet and Zircon Geochronology of the Ultra-High Temperature metamorphism: Constraints on the Rise of the Orlica-Śnieżnik Dome, 292–293. NE Bohemian Massif, SW Poland. Lithos, pp. 388–400.
Wang, J.-M., Lanari, P., Wu, F.-Y., Zhang, J.-J., Khanal, G.P., Yang, L., 2021. First evidence of eclogites overprinted by ultrahigh temperature metamorphism in Everest East. Himalaya: Implic. Collisional Tect. Early Earth. Earth Planet. Sci. Lett. 558, 116760.
Wang, Y., Zhang, L., Zhang, J., Wei, C., 2017. The youngest eclogite in central Himalaya: P–T path, U–Pb zircon age and its tectonic implication. Gondwana Research 41, 188–206.
Warr, L.N., 2021. IMA–CNMNC approved mineral symbols. Mineral. Mag. 85, 291–320.
Watson, E.B., Wark, D.A., Thomas, J.B., 2006. Crystallization thermometers for zircon and rutile. Contrib. Mineral. Petrol. 151, 413–433.
Wilke, F.D.H., O'Brien, P.J., Altenberger, U., Konrad-Schmolke, M., Khan, M.A., 2010. Multi-stage reaction history in different eclogite types from the Pakistan Himalaya and implications for exhumation processes. Lithos. 114, 70–85.
Wu, C., Zhang, L., Li, Q., Bader, T., Wang, Y., Fu, B., 2022. Tectonothermal transition from continental collision to post-collision: insights from eclogites overprinted in the ultrahigh-temperature granulite facies (Yadong region, central Himalaya). J. Metamorph. Geol. 40 (5), 955–981.
Xiang, H., Connolly, J.A.D., 2022. GeoPS: an interactive visual computing tool for thermodynamic modelling of phase equilibria. J. Metamorph. Geol. 40, 243–255.
Yakymchuk, C., 2023. Prograde zircon growth in migmatites. J. Metamorph. Geol. 41, 719–743.
Yakymchuk, C., Brown, M., 2014. Behaviour of zircon and monazite during crustal melting. J. Geol. Soc. London. 171, 465–479.
Yin, A., 2006. Cenozoic tectonic evolution of the Himalayan orogen as constrained by along-strike variation of structural geometry, exhumation history, and foreland sedimentation. Earth. Sci. Rev. 76, 1–131.
Zack, T., Kronz, A., Foley, S.F., Rivers, T., 2002. Trace element abundances in rutiles from eclogites and associated garnet mica schists. Chem. Geol. 184 (1–2), 97–122.
Zhang, G., Wang, J., Webb, A.A.G., Zhang, L., Liu, S., Fu, B., Wu, C., Wang, S., 2022. The protoliths of central Himalayan eclogites. GSA Bulletin 134, 1949–1966.
Zhang, G., Wu, C., Wang, Y., Zhang, L., Webb, A.A.G., 2024. Rapid heating (<2 Ma) to ultrahigh-temperature metamorphism via asthenospheric upwelling. Sci. Adv. 10 (24), eadl4381.
Zhang, J., Guo, L., 2007. Structure and geochronology of the southern Xainza-Dinggye rift and its relationship to the south Tibetan detachment system. J. Asian Earth. Sci. 29, 722–736.